Examining the Dynamic Response of a Floating Bridge Subjected to Simulated Traffic and Waves

Ruben Hopland Cannistraci

SUPERVISOR(S)
Jian Dai
Charoru Lu (assist)

IN COLLABORATION WITH:
Xu Xiang, Statens Vegvesen

SUMMARY

This study delves into the dynamic interaction between traffic loads, wave loads, and the vertical motion of a floating bridge. By developing an intricate coupled SIMO-RIFLEX model in SIMA and running an intelligent drive model algorithm with Python, we were able to generate realistic simulated traffic loads and wave conditions. This led to intriguing insights. The findings reveal a nuanced interplay: the mass of vehicles exerts a more significant influence on the bridge's vertical motion than their speed. Even more compelling is the influence of the wave condition. In a calm sea, the mass-induced motion increases when the mass of the vehicles is increased, but surprisingly, in a wavy sea condition, the additional traffic mass actually reduces the overall motion of the bridge. This fascinating project sheds new light on the complex factors affecting the performance and stability of floating bridges.

KEYWORDS: Floating bridge, Traffic Simulations, Structural Engineering, Naval Engineering, Pontoon bridge
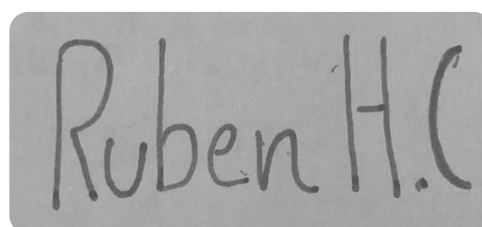
PREFACE

This master's thesis on floating bridges was written in cooperation with the Department of Civil Engineering at OsloMet. The work was undertaken in the spring, from January 15 to May 25, 2023.

A literature review was conducted in the autumn of 2022. This project was initially designed to investigate and conduct CFD simulations on pontoons. However, as the topics were adjusted to better align with the scope of structural engineering, much of this preliminary work was not incorporated into the final thesis.

The focus of this thesis is an exploration of the vertical response of a long, straight, floating bridge when subjected to traffic and environmental loads. This project draws upon an early bridge model design from 2016, intended for crossing the Bjørne Fjord as part of the Ferry Free E39 project. This project was conducted in collaboration with the Norwegian Public Road Administration (NPRA).

Before I begin, I must express my gratitude to my supervisor, Jian Dai, who has been instrumental in the execution of this project. His assistance in troubleshooting the model, and guidance on modeling were invaluable; this project might not have been achievable without him. I would also like to thank Xu Xiang, representing Statens Vegvesen, for an excellent collaboration and many insightful contributions. My gratitude extends to Chaorulu Lu for his assistance with the traffic model. Finally, I want to thank my fellow students for the amazing years at the University of Oslo Met.

Oslo, Mai 25, 2023

Ruben Hopland Cannistraci

SUMMARY

This thesis forms part of the Ferry-Free E39 project, which seeks to reduce travel time and replace ferry connections along Norway's western coast. The project plans to replace seven ferry connections with alternative crossingss. A fjord 4500 meters wide named Bjørnefjoren was considered in this thesis. Since the fjord is too deep and wide for conventional bridge designs, a floating bridge design where chosen. Two main designs have been developed: a curved bridge selected for further devolopment and a straight bridge with side anchoring.

In this project, the vertical responses of the girder and pontoons subjected to wave and traffic conditions were investigated using a SIMO-RIFLEX model. To simulate realistic traffic flow conditions, an Intelligent Drive Model (IDM) was coded in Python to generate authentic load sequences. This setup allows for large deformations, typical of long slender structures, and accommodates realistic environmental loads including wave, wind, and current simulations.

The primary objective of this study is to explore how the bridge's vertical motion is influenced by incoming waves and varied traffic conditions, achieved through two distinct parts. First, a parametric study was conducted under calm sea conditions to develop an understanding on how individual vehicle parameters such as mass and speed, affected the bridge's vertical motion. Results suggested a linear relationship between vehicle mass and vertical motion, in addition it can be seen that the bridge is more responsive to changes in mass than speed.

Since traffic flow is inherently random, a stochastic analysis was conducted to study the bridge's response under different traffic conditions. Simulations were run for free flow, capacity, and congested traffic flow under wave conditions, along with a free flow simulation under calm sea conditions. The results show that free-flow traffic resulted in the greatest vertical motion, most of which was attributed to wave response. Additionally, the results suggest that the mass of the traffic increases the bridge's inertia, making it less responsive. It should also be noted that congested flow led to a significantly greater draft.

In summary, under calm sea conditions, greater mass and traffic increase bridge motion. However, in wavy conditions, the mass of the traffic appears to stabilize the bridge. Floating bridges are complex structures subjected to complex load conditions. This project underscores the utility of numerical models in addressing complex engineering challenges.

SAMMENDRAG

Denne oppgaven er en del av prosjektet Fergefri E39, som har som mål å redusere reisetiden og erstatte fergesamband langs Norges vestkyst. Prosjektet planlegger å erstatte syv ferjesamband med alternative kryssingsmetoder. En fjord 4500 meter bred ved navn Bjørnefjoren ble vurdert i denne oppgaven. Siden fjorden er for dyp og bred for konvensjonelle brudedesign, velges et flytebrodesign. To hovedbrodesign har blitt utviklet: en buet bro valgt for ytterligere forbedring, og en rett bro med sideforankring.

I dette prosjektet ble de vertikale responsene til spenn og pontonger utsatt for bølge- og trafikkforhold undersøkt ved hjelp av en SIMO-RIFLEX-modell. For å simulere realistiske trafikkflytforhold ble en Intelligent Drive Model (IDM) kodet i Python for å generere autentiske lastsekvenser. Dette oppsettet tillater store deformasjoner, typisk for lange, slanke strukturer, og har plass til realistiske miljøbelastninger, inkludert bølge-, vind- og strømsimuleringer.

Hovedmålet med denne studien er å undersøke hvordan broens vertikale bevegelse påvirkes av innkommende bølger og varierte trafikkforhold, oppnådd gjennom to forskjellige deler. Først ble en parametrisk studie utført under rolige sjøforhold for å utvikle en forståelse av hvordan individuelle kjøretøyparametere, som masse og hastighet, påvirket broens vertikale bevegelse. Resultatene antydet et lineært forhold mellom kjøretøyets masse og vertikal bevegelse. Resultatene viser at broen er mer mottakelig for endringer i masse enn hastighet.

Siden trafikkflyten er iboende tilfeldig, ble det utført en stokastisk analyse for å studere broens respons under forskjellige trafikkforhold. Simuleringer ble kjørt for fri flyt, kapasitet og overbelastet trafikkflyt under bølgeforhold, sammen med en fri flytsimulering under rolige sjøforhold. Resultatene viser at fri flyt av trafikk resulterte i den største vertikale bevegelsen, hvorav det meste skyldtes wave respons. I tillegg tyder resultatene på at trafikkens masse øker broens treghet, noe som gjør den mindre responsiv. Det skal også bemerkes at overbelastet strøm førte til et betydelig større trekk.

Oppsummert, under rolige sjøforhold, øker større masse og trafikk brobevegelsen. Men under bølgete forhold ser det ut til at trafikkmassen stabiliserer broen. Flytebroer er komplekse konstruksjoner utsatt for komplekse belastningsforhold. Dette prosjektet understreker nytten av numeriske modeller for å takle komplekse ingeniørutfordringer

Content

Chapter 1 Table of Contents

Nomenclature

FEM	Finite element model
F_d	Drag force
DM	Dynamic Model
Aij	Frequency dependent added mass
Bij	Potential damping
Cd	Drag Coefficient
F_c	Current load
A_p	Projected area pontoons
W	Distributed Load
Fd	Drag force
A	Areal
U	Flow velocity
Φ	Velocity potential
λ	Wavelength
T	Period
f	Frequency
V	volume of body
$\dot{u}$	Fluid acceleration
C_a	Added mass coefficient
S_w	Wetted surface
I	Moment of inertial
E	Modulus of elasticity
W(x)	Curvature
EI	Flexural rigidity
M_s	Structural mas
C_s	Structural damping coefficient
C_H	Hydrodynamic damping coefficient
F_i	Inertial forces

C_m	Inertial coefficient
A(w)	Frequency dependent added mass
B(w)	Damping
C	Hydrostatic storing matrix
F(t)	Moving load
x	Position as a function of time
E	Modulus of elasticity
I	Second moment of inertial
$Kaxial$	Axial stiffness
$Kflexural$	Flexural rigidity
δmax	Deflection
Mx	Moment as a function of distance

Chapter 2 Introduction

2.1 Intro

Floating bridges are popular solutions for fjord and lake crossings due to their adaptability and cost-effectiveness. They have gained a great interest in areas where deep, wide bodies of water are present such as Norwegian fjords. In these scenarios, traditional tunnels or fixed bridges would be too expensive and difficult to construct. The "Ferry free E39" project aims to reduce travel time and improve connectivity between towns and cities on the west coast by replacing ferry crossings with other alternatives. The design of a floating bridge presents a unique set of challenges. It must be designed strong enough, to withstand both environmental loads like; wind, waves, and current loads in addition to traffic. In many cases, bridges collapse and fail due to dynamic loads from wind, where resonance is a leading cause in contrast to the static response. In the modern era, structural engineers often deal with this type of problem with numerical models.

The aim of this thesis is to study the dynamic response of a long straight floating bridge, subjected to waves and traffic to help enhance safety, reliability, and sustainability. The thesis will use an advanced numerical model to simulate and investigate the vertical motion of a floating bridge girder, considering the loads from both the environment and traffic. What is unique about this project is that an Intelligent drive model (IDM) is used to generate traffic. This model controls each vehicle on an individual level. Vehicle properties such as acceleration, distance, and speed could be chosen by the operator. It allows for the creation of realistic traffic conditions.

2.2 Background

In recent years, there has been a growing interest in improving the transportation infrastructure in Norway, particularly in the coastal highway E-39 between Kristiansand and Trondheim. The Norwegian government's "National Transport Plan 2014" highlights the need to replace all seven ferry connections along this highway. It is estimated that the new E- 39 will cut travel time in half (Gundegjerde, 2017). Furthermore, replacing these ferry connections would allow emergency vehicles to pass through much faster, which could potentially have significance for public safety. In addition, there is a possibility that an improved transport infrastructure would lead to stimulating economic growth on the Norwegian west coast.

One of the ferry crossings that the Norwegian Public Road Administration (NPRA) has been working on, is the Bjørnefjorden. This fjord is deep and wide. Two designs were initially considered: a curved and a straight-side anchored bridge (SSAFB). While both designs had their merits, the curved bridge where selected for further development by the engineering group AMC (A.Aas-Jakobsen AS, Multiconsult Norge As, COWI AS). However, this thesis will focus on the SSAFB design which presents its own set of unique engineering challenges and considerations.

2.3   Research problem

Numerical models have proven essential in solving complex engineering problems including those related to floating bridge design. These models can be used to analyze a range of factors such as statics, vibrations, aerodynamics, fatigue, and hydrodynamics. However, while there is a lot of research available on individual topics there is still a significant gap when it comes to combining them with coupled models.

In this thesis, I try to address this research gap by conducting simulations of a coupled structural and hydrodynamical model, with realistic generated traffic loads. While there is some research on the topics of moving load on floating bridge (Fu & Cui, 2012; Miao et al., 2021; Zhang et al., 2008) the topic with coupled models and realistic traffic conditions is still unexplored. For instance, some studies have shown a relationship between speed and vertical displacement where higher speeds lead to greater displacement (Fu & Cui, 2012). Another study pointed out the relationship between mass and displacements, the study found that higher mass lead to more displacement (Miao et al., 2021) .On the other hand, all these studies are using simple moving load analysis an non-uses realistic traffic.

 As a result, there is a need for more comprehensive research on numerical models that can accurately simulate the complex interaction between traffic, waves on the bridges we encounter in the coastal regions. By developing and validating a numerical model with these capabilities we can help improve transport and infrastructure design, safety, and sustainability. Overall, the aim is to contribute to the overall understanding of the behavior of floating bridges under simulated conditions. A research question were introduced to answer this.

What is the relations ship between traffic loads, waves, and vertical deflection?

2.4 Research objectives

To address the research question, several studies are conducted to study the bridge response to different traffic conditions, and environmental loads. The study is divided into two sections with different objectives. The first section is a sensitivity analysis that investigates how different vehicle properties affect the vertical deflection of the bridge girder and is measured in millimeters. The second section is a stochastic analysis that examines the deflection of the bridge girder in three different traffic scenarios, including free flow, capacity, and congestion. In addition, two more studies were conducted. One study examines the effect of waves on the vertical response of the bridge, while the other constructed a worst-case scenario based on the data obtained from the parametric study.

This research provides deep insights into the relationship between bridge deflection, traffic, and waves. Findings could be used to create safer, cheaper, and more sustainable bridge designs. Additionally, the results can inform the development of guides for using the bridge, such as speed limits in relation to ocean conditions and recommendations for when to close the bridge in severe weather.

Parametric study of individual vehicle parameter

- Effect of mass: Three simulations with the mass of 1 ton, 25 tons, and 50 tons are conducted. Vehicles travel at 110 km/h in free-flow conditions. Only one type of vehicle is included.
- Effect of speed: Two simulations where the vehicle speed is 55 km/h, and 110 km/h are conducted. Free flow conditions are applied, car mass is 1 ton, and trucks are 25 tons.

Stochastic analysis

- Three three-hour simulations of regular traffic with and without waves. Car and truck parameters are 110 km/h, 1 ton, 90km/h, and 25 tons. Scenarios such as free flow, capacity, and congestion are simulated. The vertical response is measured in meters.
- Waves characteristics are based on the annual biggest return wave

2.5 Scope and limitations

In this study, the following scope and limitations apply:

- Due to time constraints and the task's scale, all pontoons are assumed to have the same hydrodynamical and structural properties and are based on the diamond shape steel ponton design. However, this should not affect the results of the study in a negative way.
- Pontons are modeled as 6 DOF SIMO bodies
- The structural model used in this project only represents the "low section" of the bridge, excluding the cables stay bridge section and the transition section.
- All sections of the bridge girder are assumed to have the same structural properties.
- Traffic is simulated as moving points loads acting without mass.
- Only two types of traffic vehicles are considered in the traffic flow simulation. Trucks and cars.
- In this study, we will only study the vertical response of the bridge girder, ignoring the transverse and horizontal movement
- One-wave conditions are simulated. This condition is based on the annual large return wave with a height of 1.6 meter.
- Wind and current effects are neglected, wind could play a significant role, but the current has been proven to not affect the vertical motion

2.6 Structure of Report

Chapter 1: In Chapter One, you will get a brief introduction to the floating bridge problem. Topics like intro, background, research gap and model limitations

Chapter 2: Background on floating bridges. This chapter provides historical background on floating bridges, typical design, and key features and elements of a floating bridge

Chapter 3: Theoretical Framework. This chapter presents the theoretical concepts used in the project, including hydrodynamics, structural and traffic fundamentals. The simplifications used are also discussed.

Chapter 4: Creating model of pontoon in WADAM, conducting hydro analysis

Chapter 5: Creating a coupled structural and hydrodynamical model with SIMO-RIFLEX

Chapter 6: Discretizing the bridge, simulation parameter, traffic model

Chapter 7: Results. This chapter presents the results of the simulations conducted in the project and provides a brief explanation of the findings.

Chapter 8: Conclusion. This chapter provides a discussion of the results.

Chapter 3 Background on floating bridges

3.1 What is a floating bridge?

A floating bridge, commonly referred to as a pontoon bridge, is a type of bridge structure designed to provide a passage over the water by utilizing pontoons as its foundation. These large floating bodies generate buoyancy by displacing water, this effect is used to support its weight. The bridge girder is a key component that supports the deck by carrying the loads from traffic, wind, etc., from the spans to the columns. Columns transfer loads to the pontoons, which act as a foundation in a regular bridge.

To ensure stability, the pontoons are restrained with a set of mooring lines to hinder horizontal motion. The lines transfer the horizontal forces from the pontoons to the anchors. Anchors provide safe and strong connections to the seabed.

3.2 History of floating bridges

Pontoon bridges have been utilized for centuries to cross rivers, lakes, and other bodies of water. Throughout history, both the military and civil society have shown great interest in this type of structure. One of the earliest documented floating bridge designs was developed in China during the 8th and 9th centuries BC, with the construction of the first permanent bridge around 200 BC. The Persian king was also interested in this structure. In 481 BC, he constructed a 1.3 Km long ponton bridge to enable his army to cross could cross the Hellespont strait. These examples demonstrate the historical use.

3.3 Military use of floating bridges.

Floating bridges have long been favored by the military due to their numerous advantages in military operations. Some of these benefits include they are quick and easy to construct, assemble, and disassemble. Off-site manufacturing capabilities, as there are fewer opportunities for safe construction. Reusability, they could easily be dismounted, transported to a new location, and reassembled again. shows the Ribbon bridge system used in an exercise " DEFENDER – Europa 22" (Porter, 2022). Standards build time for bridge is 23 minutes (U.S. Defense, 2022)
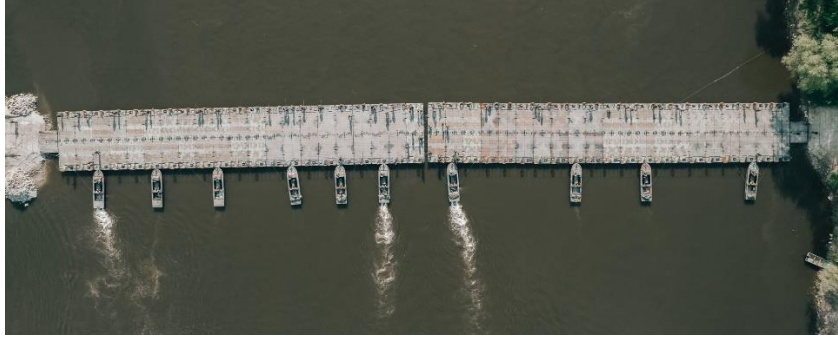
Figure 1: Ribbon bridge system across Vistula River in Polan (Michal Czornij, US Army)

3.4   National and International floating bridges

In this section, several examples of floating bridges will be presented. First, two arch bridges that are located in Norway will be discussed, followed by a straight bridge from the US.

Bergsøysundet

Constructed in 1992 between Aspøy and bergsøya, the Bergøsysundet Bridge serves as a passage for traffic, pedestrians, and bikes between the islands. Seven pontoons support the weight of the structure, consisting of a truss system formed as an arch spanning over 930 meters. Both ends are fixed. The main span measures 106 meters.

Figure 2: Steel-truss-system, concrete pontoons, and fixed ends (Kjell E 2016, FOURSQUARE)

A key feature of this bridge is its arch design. Arches are well-studied and often used in bridges with long spans and no possibility for support in the middle sections. When constructed correctly, arches effectively reduce tension and mitigate buckling. Instead, they transfer loads

as compression forces. Forces are then distributed to the ends. The Romans' engineers knew about this and used this principle to build huge structures like Pantheon and the Acqvaducts.
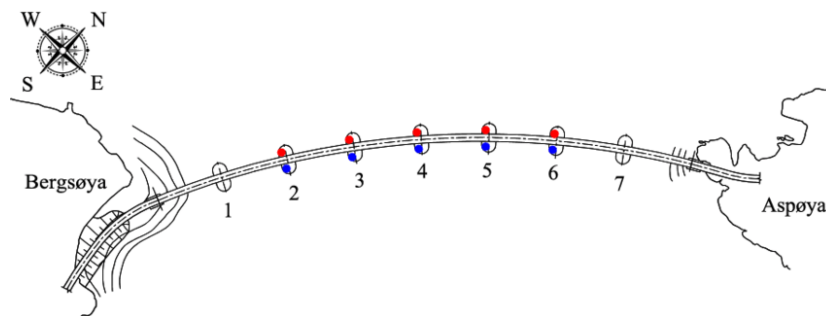
Figure 3: Top view of arch bridge

Nord Hordaland Bridge

Constructed in 1994, the Nord Hordaland Bridge is the second pontoon bridge in Norway, connecting Flatøy and Bergen. A combination of two structural systems was employed to meet the design criteria. An arched pontoon bridge section standing on ten pontoons was combined with a cable-stayed bridge. The cable-stayed bridge would provide a passage for boats. Currently, it holds the title of Norway's longest pontoon bridge, with a span length of 1,614 meters.

Figure 4: Nord Hordaland Bridge (broer.no)

A key feature of the Nord Hordaland Bridge is the combination of two structural systems, which allows for efficient load distribution and accommodates maritime traffic. A similar design is used in the bridge we study

Evergreen Point (520 Bridge)

Opened to the public in 1963, the Evergreen Point Bridge, also known as the 520 Bridge, connects two lake banks over a distance of 2,350 meters. This straight-side anchored pontoon bridge utilizes 77 pontoons to support the structure and currently holds the record for the longest floating bridge.

Figure 5: Evergreenpoint bridge (Wikipedia)

A key feature of the Evergreen Point Bridge is its side-anchored design, which sets it apart from the Bergsøysundet and Nord Hordaland bridges. Due to its long and slender structure, the bridge is prone to large bending moments. To counteract this, a series of mooring lines are attached to the sides, effectively shortening the span and transferring horizontal forces from the bridge to the seabed, where various anchors are employed.
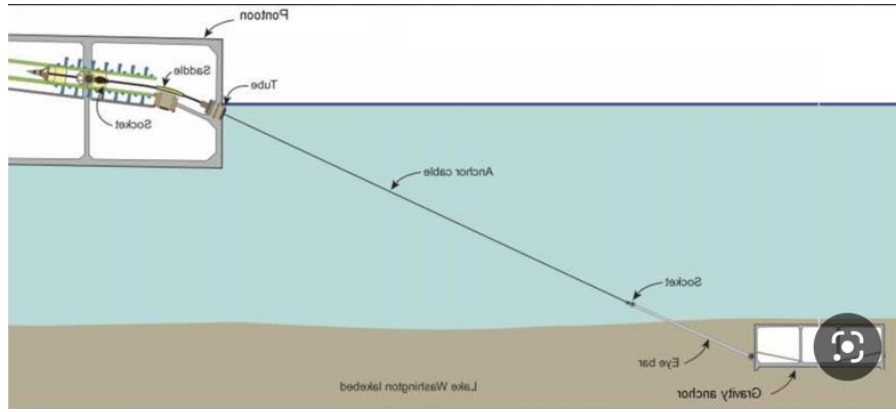
Figure 6: Gravity-anchor, mooring lines for 522 bridge (research gate, Sergio Tattoni)

The Evergreen Point Bridge's unique design showcases an alternative approach to floating bridge construction, emphasizing the importance of anchoring and stabilization in such long-span structures.

Chapter 4 Theoretical framework

This chapter provides an overview of the theoretical framework, mathematical models and model theory used to build the model and simulate different load. The aim is to help the reader understand how the models are made, such that the principals and methods could be replicated for another study or, design experiments with different theory to further validate the findings.

The chapter is divided into several sections, each section focusing on different aspects of the floating bridge beginning with a section discussing different loads that may be considered. The next sections describes the hydrostatic and hydrodynamic fundamentals on the pontoons. Topics like drag, buoyancy, waves, added mass, and damping will be disused. Then, a section describing the structural modeling is presented, with topics like beam properties, dynamic responses, eigenvalues, etc will be discussed, and next a section about traffic modeling, in this section, a short description of how the traffic model works, and how it is implemented is given. Lastly, the different analyses are discussed.

This chapter provides info on many different independent topics like hydrodynamics, structural dynamics, and traffic simulation. Floating bridges are complex structures, and a multi-disciplinary understanding of topics is required to create valid models. This chapter should provide the reader with a solid foundation.

4.1 Defining typical loads

In this section, a presentation of typical loads that must be considered for floating bridge designs. Beginning with a general list covering the most common loads. Followed by, the project-specific loads are discussed in detail in their own sections.

Typical load on floating bridges

- Dead load (self-weight)
- Live loads (traffic)
- Impact loads
- Wind loads
- Current loads

- Longitudinal forces due to vehicle acceleration or deceleration
- Centrifugal force due to vehicles changing lateral direction, curved bridges are more prone thot this.
- Wave loads
- Current loads
- Marine growth
- Thermal loads
- seismic loads
- Centrifugal force
- Snow loads
- Accidental loads
- Loads due to tidal variation.

Dead load

Dead loads are all permanent loads resulting from bridge elements, often referred to as self-weight. This includes the weight of all bridge components, such as, asphalt, concrete, steel, permanent ballast, mooring lines, tower, cable railings, and other equipment. The resulting forces act in the vertical direction.

4.2 Hydrodynamic and hydrostatic effects on pontoons

Pontoons are subjected to hydrodynamical and hydrostatic effects; this chapter provides info on the modeling theory and simulation theory. As the pontoons float in water, environmental effects such as waves and currents must be accounted for properly. This section includes topics like wave-model, current model, diffraction forces, radiation forces, added mass, damping, drag, Morrison equation, and simulation tools.

In this project, all hydrodynamic models rely on potential flow solvers (PFS) based on second-order potential theory. During the initial stages of the project, alternative methods, such as Computational Fluid Dynamics (CFD), were investigated and compared. However, the increased accuracy that CFD could provide was deemed unnecessary for the scope of this study. Moreover, CFD demands significantly more time and computational resources, which were not available for this project. As a result, potential flow solvers were chosen as the most suitable option for modeling hydrodynamic loads in this context.

Potential flow theory

Potential flow theory is a part of fluid dynamics considering a particular type of flow, classified as ideal flow. The underlying assumptions are conserved of momentum (inviscid flow), conservation of mass (incompressible flow), and irrotational flow (no curl). For the pontoon – water interaction, this criterias are largely valid. However, the PFT does not account for effects such as vortices, turbulence and skin friction drag. The primary focus of this study is to investigate the wave-traffic, particularly the traffic aspect. Therefore, this effect does not play a vital role and can be neglected. However, a Morrison model was implemented to solve for viscous drag forces (Techet, 2005).

$$\nabla \times u = 0 \tag{4.1}$$

$$u = \nabla \Phi = \frac{\partial \Phi}{\partial \mathrm{x}} i + \frac{\partial \Phi}{\partial \mathrm{y}} j + \frac{\partial \Phi}{\partial \mathrm{z}} k \tag{4.2}$$

$$\nabla \times \nabla \Phi = 0 \tag{4.3}$$

$$\nabla * u = 0 \tag{4.4}$$

Current load

Current flows around the pontoons and generate drag forces in opposite direction of current motion. The drag coefficients are   obtained from SSV estimates presented in their documentation. In this project the quadratic formula is used (*equation 4.5*), this was recommended in DNV manuals. For this project the currents are caused by tidal variation and wind. Values are obtained from analysis done by SSV.

$$F_D = \frac{1}{2} * \rho * C_d * A_p * u^2$$
4.5

- F_D Drag force
- C_d is the drag coefficient
- U is the current velocity

Morisons's equation

The Morison equation was implemented to improve realism by including viscous forces. This equation gives the total drag force (F_T) as the sum of inertia-forces (F_I) and the drag forces (F_D).

$$F_t = F_I + F_D$$
4.6

$$F_t = \rho * C_m * V * + \frac{1}{2} * \rho * C_D * A * u * \dot{u}$$
4.7

- C_m is the

Inertial forces consist of Froude-Krylov forces and added mass, represented by the first term. Added mass is already discussed. The Froude – Krylova force accounts for the force arising from the pressure generated by the undisturbed wave acting on the pontoon surface.

$$F_I = \rho * C_m * V * \dot{u}$$
4.8

$$F_I = \rho * V * \dot{u} + \rho * C_a * V * \dot{u} \qquad\qquad 4.9$$

C_a is the

Irregular wave model JONSWAP

In real- word scenario, waves are rarely regular or periodic, meaning they exhibit varying height and period. To accurately model the ocean environment we must consider irregular waves. Irregular waves are modeled as sums of regular sinusoidal waves with different characteristics. Irregular waves are often described in a statistical manner. A specter is used to describe the distribution of energy with respect to frequency.

In this project a JONSWAP (Joint North Sea Wave Project) spectrum is used to model the waves. This spectrum is commonly used for wind-generated and was developed in the 1970s, based on observations in the North Sea. It is an Empirical relation(Hasselmann

T.P.Barret

E.Bouws

H.Carlson, 1973).

$$S(\omega) = \frac{\alpha * g^2}{\omega^5} exp\left[-\beta \frac{\omega_p^4}{\omega^4}\right]\gamma^\alpha \qquad\qquad 4.10$$

- α is related to windspeed
- ω is wave frequency
- ω_p is wave-frequency
- g is gravity

Diffraction forces

Diffraction forces are hydrodynamic forces arising when waves encounter change in depth or an obstacle, such as pontoons. Since the pontoons are in deep water, only the effect of wave

bending must be considered. When the waves bend, they exert a pressure on the pontoon's surface that must be accounted for.

The first order diffraction effect is calculated in a software called Wadam, based on potential flow theory. Results are added to the wave excitation transfer functions, it should be added that other effects add to these functions. For this thesis Wadam is only running frequency - domain simulations. (DNV-GL, 2017)
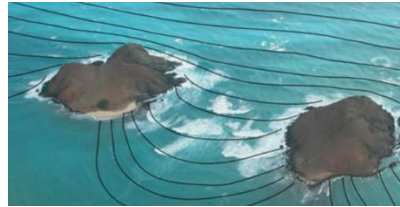
Figur 1: Wave diffraction, taken from the YouTube film 1min 42s "Wave refraction"
https://www.youtube.com/watch?v=E9UJjdlTQQI

Radiation Forces

Radiation forces are the forces that emerge when pontoons oscillate in calm water conditions. These forces occur as the pontoons transfer energy to the surrounding water, generating waves and transmitting momentum from the body to the water through various mechanisms. There are three primary types of radiation forces: hydrodynamic mass (also known as added mass), damping force, and restoring forces. The expression for these forces can be found below. (Lewandowski, 2004)

$$-\omega^2 \left(M + A(\omega) \right) i\omega \left(B(\omega)_p \right) + C + = F(\omega, \beta) \qquad 4.11$$

Added mass

Added mass is a part of the hydrodynamical loads affecting the pontoons and must be dealt with. It is particularly important to consider the effect of added mass when structures are subjected to oscillatory motion. This is the case for pontoons. The effect is dependent on geometry, oscillation frequency, and forward speed (O.M.Faltinsen, 1999).

Added mass can be understood as pressure acting on the surface of the pontoon because of the acceleration of surrounding liquid. Only the water surrounding the pontoons contributes to this force, the ballast water and other internal pockets are considered separately. Added mass causes an increase in virtual mass, increasing inertia.

$$F_{inertia} = a * (m + m_a)$$
4.12

- m_a is added mass
- m is the mass
- a is acceleration

WADAM calculates added mass by solving the equations of motion (*equation 4.2*) for various wave frequencies and heading angles. Firstly, a frequency-dependent added mass is computed based on potential flow theory. Subsequently, Morison's equation is employed to determine a frequency-independent added mass. It should be noted that in this thesis, there is no current interaction. For more info read in the User manual Wadam (DNV-GL, 2017).

$$-\omega^2 \, (M \, + \, A(\omega)) \, i\omega \, (B(\omega)_p \,) \, + \, C + \, = \, F(\omega, \beta)$$
4.13

- M is 6x6 inertial matrix
- $A(\omega)$ is the 6x6 frequency-dependent added mass matrix
- $B(\omega)_p$ is the frequency-dependent potential damp matrix
- C is the hydrostatic stiffness restoring matrix
- $F(\omega, \beta)$ is an exciting force vector

$$M_A = \begin{bmatrix} m_{11} & 0 & m_{13} & 0 & m_{15} & 0 \\ 0 & m_{22} & 0 & m_{24} & 0 & m_{26} \\ m_{31} & 0 & m_{33} & 0 & m_{35} & 0 \\ 0 & m_{42} & 0 & m_{44} & 0 & m_{46} \\ m_{51} & 0 & m_{53} & 0 & m_{55} & 0 \\ 0 & m_{62} & 0 & m_{64} & 0 & m_{66} \end{bmatrix}$$

Figure 7: Added mass matrix

Hydrodynamic damping

Hydrodynamic damping refers to the forces acting on oscillating structures in water, such as pontoons, causing forces in the opposite direction of motion and draining the system for energy. These forces can be divided into two main terms: viscous damping and potential damping. Potential damping is the energy lost to wave-making (radiation), while viscous damping is caused by skin friction, wave drift, vortex shedding etc (Fossen, 1994). Viscous damping generally contributes to a larger force than potential damping; however, empirical methods, CFD, or scale models have to be used to obtain the coefficients.

Damping models used for pontoons

WADAM calculates damping using various methods, including frequency-dependent damping from potential theory and frequency-independent linearized viscous damping from Morison's equation. For our project, we will incorporate both types of damping. A 6x6 matrix represents the linear damping, while the frequency-dependent damping is represented by a function (DNV-GL, 2017).

In general, potential flow solvers typically only solve for frequency-dependent damping. However, we can obtain viscous damping by including a Morison term in our analysis. It is important to note that the results for viscous damping obtained through this approach may not be as accurate as those derived from computational fluid dynamics (CFD) simulations.

Hydrostatic Stiffness

Hydrostatic stiffness refers to the forces acting on the pontoons' submerged area. These forces counteract vertical displacement and angular rotation. For this project, the main concern is the hydrostatic stiffness in the vertical direction, also called buoyancy. Hydrostatic stiffness values are used to calculate the equilibrium position and vertical displacement when the bridge is subjected to traffic and waves.

WADAM is used to do a hydrostatic analysis, which includes: the center of buoyancy (COB), water plane area (WPA), metacenter height, and global restoring matrix, which is a 6x6 matrix. Wadam uses the total displaced volume based on a panel model to calculate this parameter. The equation (equation 3.5), also known as buoyancy, obtains the hydrostatic stiffness data in

the vertical direction. Read the WADAM User manual (DNV-GL, 2017) for more info on the other hydrostatic parameters.

$$C_{33} = \rho * g * S \qquad\qquad 4.14$$

- C_{33} is the hydrostatic stiffenes coefficient
- ρ   is the density of seawater.
- S   is the surface area of the pontoon seen from above

RAO's: Respons Amplitude Operator

The response amplitude operator is a term used to describe the hydrodynamic response of a floating structure. A spectrum is used to describe the response with respect to frequency. The spectrum can divide into three distinct areas, representing motion dominated by hydrostatic stiffness, damping, or mass.

1. In the first region, the motion is governed by hydrostatic stiffness or restoring force. For pontoons in this region, the hydrostatic stiffness is significant compared to the mass, causing the pontoon to follow the wave motion closely.

2. The second region is characterized by the natural frequency domain, where high resonance and considerable damping occur. In this region, the pontoon's response to wave excitation can be amplified, and adequate damping is crucial to prevent excessive motion or even damage to the structure.

3. The third region corresponds to the high-frequency domain, where mass terms dominate. In this region, the waves have a diminished effect on the pontoon, as its mass helps to stabilize the structure against the wave-induced motion.

Understanding the various regions in the RAOs enables engineers to design pontoons that offer optimal stability, performance, and resilience against the wave-induced motion (Journée & Massie, 2001)To validate the hydrodynamic model, it is essential to conduct simulations of waves across all regions to ensure accurate and appropriate behavior is represented.

4.3   Bridge discretization and moving loads

This section introduces the traffic model used to realistically simulate the impact of vehicles on bridges. Traffic significantly affects bridges in terms of static, dynamic, and moving loads, as well as vibrations. In this study, traffic is modeled as moving loads with each vehicle represented by a force vector moving over the bridge. Key topics include moving loads problem, girder discretization and traffic generation.

Figure 8 Taken from "The platform" by Bruce Gray 23,8.2017

Moving loads problem

Modeling traffic accurately is challenging due to its chaotic nature. Vehicles move randomly in all directions, inducing forces and vibrations. To simplify the model, several assumptions were made:

- Movement is restricted to X-axis
- Only gravitational forces are accounted considered.
- Reduced loading is used. Each vehicle is represented by a single force.
- All vehicle loads are located on the center line. Moments around X and Z axis are neglected.

$$F(t) = [0, 0, -F_T(t)] \qquad\qquad 4.15$$

Discretization of bridge girder

To accommodate moving loads, the girder is discretized into a finite set of elements containing nodes where loads can be applied. Each bridge span is transformed into smaller elements with many nodes, this is illustrated on *Figure 9*. This prosses was handled with RIFLEX.
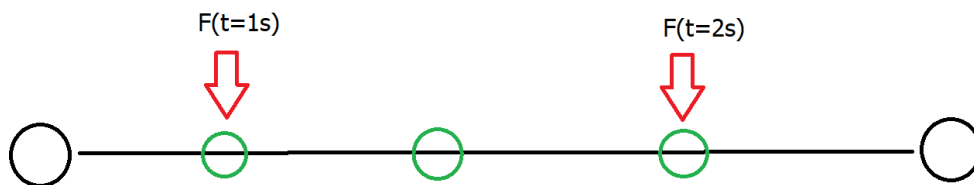

Figure 9: Discretization of beam

Discretizing the loads

In order to apply loads to the nodes, they need to be discretized. While the physical model involves continuous load movement between nodes, the software can only apply forces to nodes. A shape function transforms the physical model into a discretized version. When loads are located between nodes, the shape function divides the load into two and applies them to the nearest nodes. Each node has its own loading sequence. (Figure 11 and Figure 12). This prosses is handled with a python code and a MATLAB code, the information flow is illustrated at *Figure 11* .
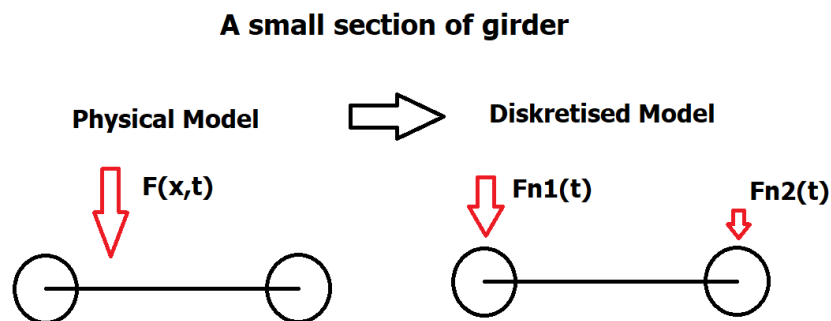

Figure 10: Illustration of physical model left, and discretized model right, the force is splitt on two nodes
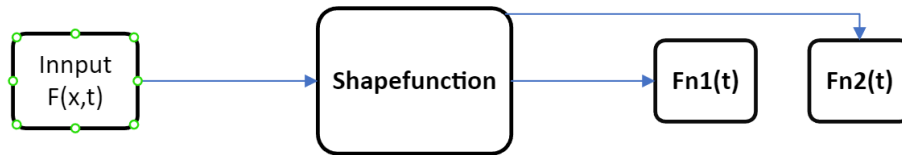
Figure 11: Flow diagram of discretization.

4.4 Traffic model

This section discusses the data flow, traffic model, and IDM.

Data flow sequence

The data flow is illustrated below. First, Python code made from Bilal Himite is used to simulate traffic on a microscopic level. Next, A MATLAB code is used to combine loads from trucks and cars and add force vectors. Lastly, a second MATLAB code generates load files for each node. These codes are taken from Jian Dai.
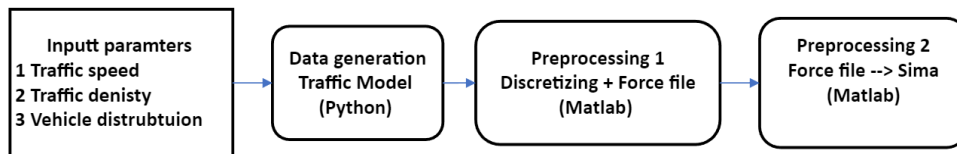

Figure 12: Data flow scheme for traffic model.

Traffic flow data generator with PYTHON

Bilal Himites Python code was chosen for traffic generation due to its traffic simulation at a microscopic level resulting in a high level of realism. This code incorporates an intelligent driving model (IDM) (Himite, 2021).

IDM

The Intelligent Driving Model (IDM) simulates realistic vehicle behavior by changing the acceleration of each vehicle based on several variables such as distance, speed, etc. The model is represented by equations *(4.9 and* 4.10*)*. This model can generate realistic traffic data representing different traffic conditions such as free flow, congestion, and capacity (Treibner,

2000). For more information, refer to Treibner's article (Treibner, 2000) and Himite's web article (Himite, 2021).

$$\frac{dv_i}{dt} = a_i \left(\left(1 - \left(\frac{v_i}{v_{0,i}} \right) \right)^1 - \left(\frac{S * (v_i \Delta v_i)}{s_i} \right)^2 \right) \qquad 4.16$$

$$S * (v_i, \Delta V_i) = S_{0,i} + v_i T_i + \frac{v_i \Delta v_i}{\sqrt{2 a_i b_i}} \qquad 4.17$$

- $S_{0,i}$ is the minimum desired speed
- $v_{0,i}$ is the maximum desired speed
- T_i is the reaction time
- a_i is the maximum acceleration
- S is the actual distance between vehicles

(Himite, 2021)

Converting data to SIMA- readable files

The traffic data is then converted into SIMA-readable files using MATLAB codes. The process involves transforming the data into moving load vectors with proper magnitude, discretizing the loads, and creating load sequences for each node.
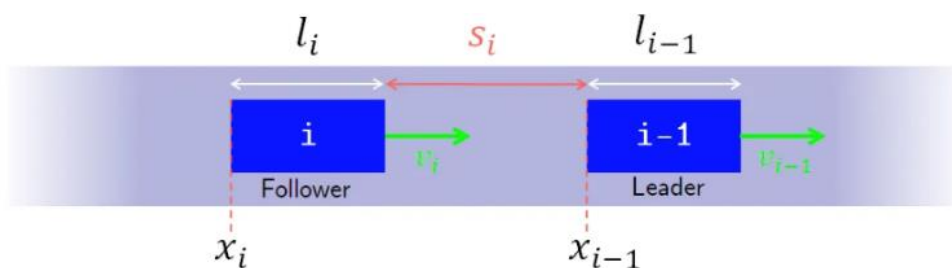

Figure 13: Illustration of IDM parameters with two vehicles

4.5   Description of Numerical methods

Finite Element Method

The finite element method (FEM) is a powerful numerical tool used to solve engineering problems. FEM was since it can handle large and complex problems.

FEM involves discretizing the object of interest into smaller, interconnected "finite elements" organized in a mesh. The method calculates the total stiffness matrix by considering the elements connections, material properties, applied loads, and boundary conditions. Subsequently, the solver solves the resulting system of differential equations. (Equation 4.18 b) is the virtual work equation expressing equilibrium. For more information read *SIMA Documentation – Finite Element Formulation (SINTEF, 2017).*

$$\text{a) } x = x(X, t) \qquad \text{2) } \int_{V_0}^{1} S : \delta E \, dV_0 = \int_{A_0}^{1} t_0 * \delta u \, dA_0 + \int_{V_0}^{1} f_0 \delta u \, dV_0 \qquad 4.18$$

x   is positions as a function of time

Riflex was chosen based on its efficiency in solving linear and non-linear FEM problems, Riflex uses a formulation called FENRIS. This formulation enables large rotations and translation commonly found in floating bridges (SINTEF, 2017)

Static analysis

To validate the model a static analysis using two independent methods: FEM and Euler-Bernoulli beam theory. The latter was chosen for its simplicity and well-documented validity for this type of problem.

The bridge girder was model ass a 2D fixed beam with a distributed load. This was valid due to the problem satisfying the criteria for Euler Bernoulli beam theory. Criteria are located below this section.

1. **Constant cross section**: For this project we assumed the cross section to be constant, this could be done since the purpose of the study was to investigate the effect of a traffic model and not the deformation itself.

2. **Beam with fixed end**: since all spans were similarly loaded, the sections connecting the two segments would as a result be horizontal, which makes the fixed end applicable

3. **Constant distributed loads:** For the static model only dead loads are include, and they

$$\delta_{max} = \frac{\omega * l^4}{384 * E * I} \qquad \delta(x) = \frac{w * x^2}{24 * E * I}(l - x)^2 \qquad M_x = \frac{\omega}{12}(6 * l * x - l^2 - 6x^2) \qquad 4.21$$
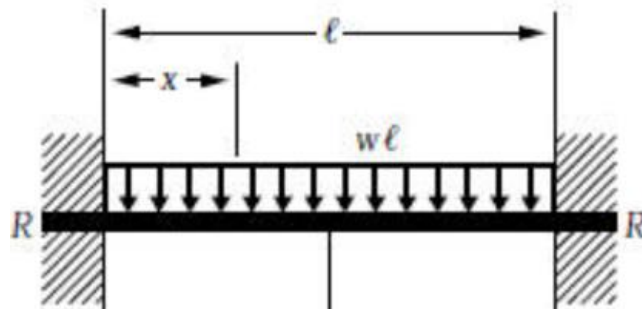
could be model as distributed load.

Figure 2: Beam fixed at both ends - Constanta distributed loads

Euler beam Equation

Euler beam equation (equation 4.19a) relates loads to deflection based on flexural modulus of elasticity and second moment on inertial, beam stiffness are taken from Statens Vegvesen (SSV, 2018)

$$a) \; \frac{d^2}{dx^2}(E.I.\frac{d^2w}{dx^2}) = W \qquad\qquad a) \;\; I = \iint z^2 \, dydx \qquad\qquad 4.19$$

I is the second moment of inertial

E is the Modulus of elasticity

W is the distributed load

$$a) \; K_{axial} = EA \qquad\qquad\qquad b) \quad K_{flexural} = EI \qquad\qquad 4.20$$

K_{axial} is the axial stiffness

$K_{flexural}$ is the flexural rigidity

δ_{max} is the deflection as a function of distance

M_x is the moment as a function of distance

Static FEM-Analysis

For the static FEM-calculations, *Equation 4.23 (a)* is solved iteratively with to purposes. First is to determine the static equilibrium, second is to determine the deformed shape and forces. Riflex code accounts for both internal and external loads.

Incremental updates of the equilibrium equation do this. Loads can be applied in several load steps. For each load step, the solver algorithm iterates until the convergence criteria are satisfied (4.23 b). This is (Equation 4.23). Each iteration should help the solution converge. Riflex uses the Newton–Raphson method to improve the converge rate (equation 4.22). It should be mentioned that Riflex uses co rotated ghost reference description, motion is related to local coordinate system at member level. All formulas are taken from *SIMA Documentation* (DNV, 2023) All formulas are taken from *SIMA Documentation* (DNV, 2023)

$$r_{n+1} = r_n - K_I^{-1}(r_n)(R_{int}\text{-R})$$ 4.22

a) $R^s(r) = R^E(r)$ b) $\Delta r_k^j = \left[\frac{\partial R_{k-1}}{\partial r}\right]^{-1} R_k^{j-1}$ c) $\frac{\|\Delta rjk\|}{\|rjk\|} < \varepsilon d$ 4.23

r is nodal displacement

$R^s(r)$ is the internal structural reaction force

$R^E(r)$ is the external force vector

Time-dependent linear FEA analysis

Structures subjected to time-dependent or cyclic loading should be analyzed in the time domain with a dynamic analysis. Traffic and waves are characterized as dynamic loads. This approach is also recommended by Cook in the book *CONCEPTS AND APPLICATIONS OF FINITE ELEMENT ANALYSIS* (Cook & S, 2001).

The dynamic analysis tool employs the same stiffness matrix found in static analysis but introduces modifications for the equation of motion (3.23). Two critical terms are integrated into the equation; an inertia term (b) and a damping term (c), both of which depend on motion. Furthermore, this equation is solved the time domain (Cook & S, 2001).

a) $[m]\ddot{u} = r_i$ b) $[c]\dot{u} = r_d$ c) $[m]\ddot{u} + [c]\dot{u} + [k]u = r$ 4.24

$[m]$ is the mass matrix

$[c]$ is the damping matrix

r_i is the internal forces

r_d is the damping forces

u is the displacement, u with a dot, and double dote is velocity and acceleration

Damping

Damping forces in this project are influenced by both structural and hydrodynamical factors. In this section, the structural contribution is discussed

Rayleigh damping is a vital contributor in nonlinear dynamic analysis, and dissipates energy from an oscillating structure, hence preventing infinite oscillation. Structural issues typically see damping forces contributing less than 10% to the total force(Cook & S, 2001).

Natural frequency, mode shape, and eigenvalues in structural engineering

The study of the floating bridge in this project involves a detailed examination of its natural frequencies, mode shapes, and eigenvalues. These critical structural parameters dictate the behavior of the structure under various load conditions and dynamic interactions with its environment. A brief discussion is located in the following sections

Natural frequencies are the inherent oscillation of a system, determined by its stiffness and mass. Structures typically have multiple natural frequencies. Understanding these frequencies is vital to mitigate resonance risks, which could lead to disastrous consequences.

Resonance, a condition where a structure is subjected to cyclic loading at its natural frequency, can lead to large deformations. Sources of such loading can include traffic, waves, wind, etc. Unchecked resonance could result in fatigue, high stress, failure, shortened lifespan, or uncomfortable vibrations for users. The effects of damping on resonance are depicted in *Figure 16.*
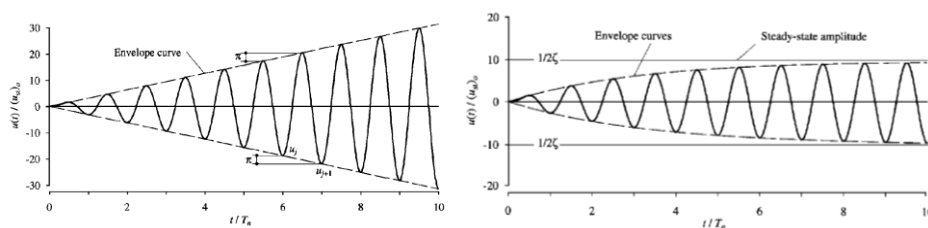

Figure 14: Response of undamped and damped system to sinusoidal loading. Taken from Dynamics of structures Theory P.66 (K

Chopra, 1995)

Mode shapes can be described as the deflected shape of a structure while resonating at a certain frequency.

In bridge floating bridge analysis, it is standard practice to include an eigenvalue analysis. This complex analysis yields a series of eigenvalues and eigenvectors that provide significant insights into the dynamic properties of the bridge. For this project, Riflex is used to conduct this analysis. The main principle is solving (equation 4.25),

a) $\omega_n = \sqrt{\dfrac{k}{m}}$
b) $\det([k] - w_i^2 M\{\emptyset\}) = 0$
4.25

ω_n is the natural frequency

K is a structural stiffness

m is the mass

Chapter 5 Pontoons

5.1 Introduction to Pontoons

Pontoons serve as a critical structural element in the design of floating bridges. They provide a stable foundation that supports the weight of the bridge segments spanning across water, thereby offering an alternative to more traditional methods like suspension bridges. The pross involved, creating a panel model in GeniE,

In this project, the pontoons' unique properties have to be captured with a separate model. This model was used to determine the hydrodynamical and mass properties of the pontoons. The process involved creating a panel model in GeniE, then using a diffraction analysis software (WADAM) to obtain the relevant data.

Wadam was chosen based on the program's capabilities of conducting simulations and analysis in the frequency domain. Its compatibility with GeniE and SIMA and its supported functions like mass calculations, wave response, added mass, and potential damping made the software qualify for this project (DNV, 2017).
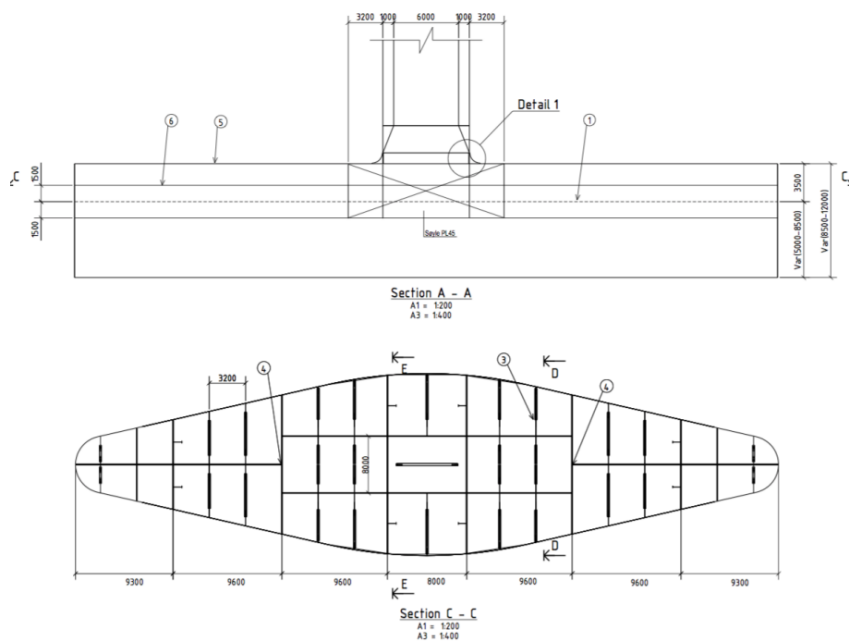
5.2 Pontoons Design and Specifications

Figure 15: Illustration of typical steel pontoon P.105" (Multiconsult, 2017a)

The structure is supported by 33 pontoons, 32 are made of steel. The steel pontoons are shaped like "diamonds," and can be categorized into two types based on their geometry: large and small. The draft and freeboard vary among individual pontoons, with typical draft values being 5 meters and freeboard values being 3.5 meters. All pontoon dimensions are listed in the Appendix.

Shape	Axis	Length [m]	Width [m]	R1 [m]	R2 [m]	Draft [m]	Freeboard [m]	Displacement [Ton]
Diamond	8 to 29	62	16	40	2,5	5	3.5	3421

Table 1: Dimensions for steel pontoons based on the table on P.105 in analysis and design (Multiconsult, 2017b)

Creating a Panel Model of Pontoons with GeniE

The process of creating a finite element model (FEM) of the pontoons was accomplished using GeniE according to the guidelines outlined in GeniE help manual *A7*. This process primarily involved transforming 2D sketches into 3D models.

Firstly, an overhead view of the pontoon's top contour was sketched in 2D on a reference plane. Following this, an offset plane was created 10 meters beneath the top of the pontoon. The choice of this distance, which exceeds the total pontoon heigh, will be explained subsequently.

The top contour was then projected onto this offset plane. Using the lines of the projected contour, surface planes were created between them and grouped together under the set named "WS1". This set of surfaces was designated as a "wet surface condition", serving as the regions where hydrodynamic interactions would take place. The mesh was chosen to 0.5 meters, this value is verified later. The panel model can be seen on (Figure 16)

A crucial step in the process was creating a "Dummy Hydro Pressure load case" referred to as "LC1". This load case was based on the "WS1" enabling WADAM to identify where hydrodynamic loads should be applied (DNV, 2021).
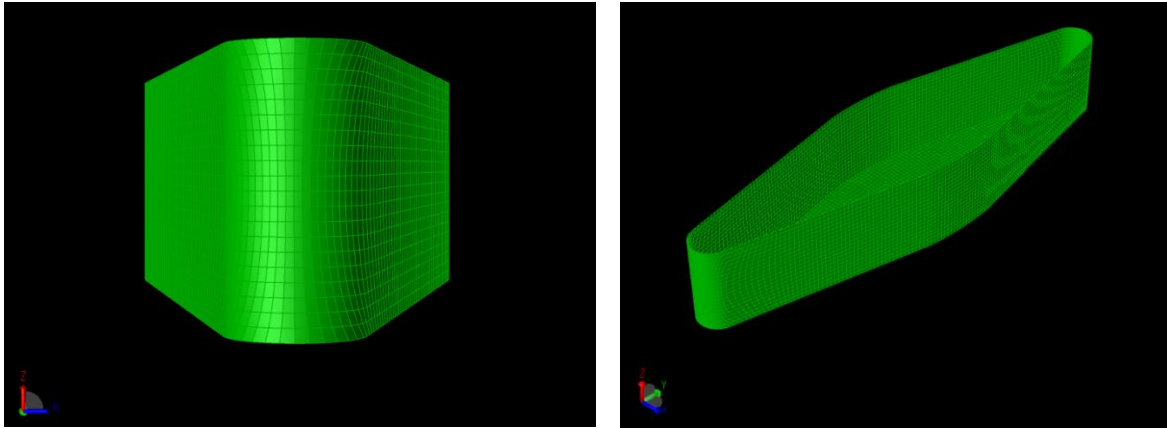
Figure 16: Panel model of pontoon with mesh size 0.5 meters,

The choice of a 10-meter heigh pontoon model was done to simplify the modeling process and reduce the workload. Despite the pontoon's drafts ranging from 5 meters to 8.5 meters, an algorithm in the Wadam adjusts the wet elements extending above the surface to align with the sea level *(Figure 17)*. This ensures that the surface above the waterline does not contribute to hydrodynamical loads (DNV-GL, 2017). This trick would allow for using the same panel model for all WADAM simulations in this project.
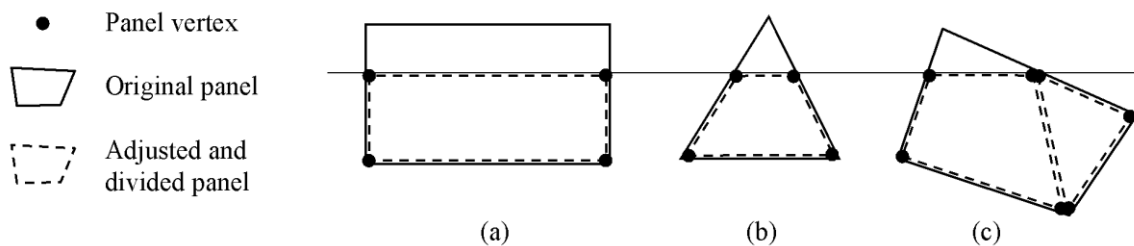
Figure 17: Illustration of self-adjusted wet elements from the WADAM user manual P.10 (DNV-GL, 2017)

The incoming wave direction was set from 0° to 90°; this could be done due to the pontoon's symmetry in both directions; the interval was set to 3°. The frequency ranged from 0.01 seconds to 100 seconds; this was sufficient to capture both the low-frequency responses and the infinity-frequency response.

5.3   Hydrodynamical analysis in WADAM

The panel models were introduced into WADAM, a hydrodynamic analysis tool that operates from the HydroD interface. For this setup, both a panel model and a point mass model were selected. The modeling process was rather straightforward, guided by the interface's step-by-step wizard.

The incoming wave direction was set from 0° to 90°; this could be done due to the pontoon's symmetry in both directions; the interval was set to 3°. The frequency ranged from 0.01 seconds to 100 seconds; this was sufficient to capture both the low-frequency responses and the infinity-frequency response. The tolerance was set at a limit of 1%.

Creating multiple panel models with different mesh size

Four panel models were created with different mesh sizes :2 meters, 1 meter, 0.5 meters, and 0.25 meters. The results were exported in the form of a .SIF file, which contained vital data such as the mass matrix, damping matrix, added mass matrix, and transfer functions.
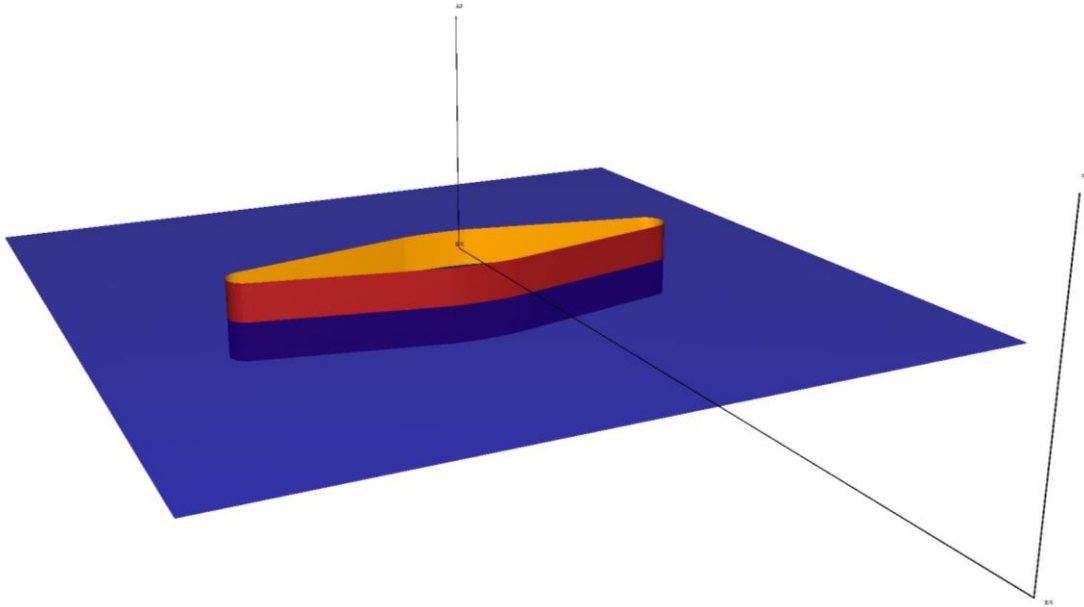
Figure 18: Panel model in WADAM

5.4 Validation tests

To build confidence in the model, validation tests were conducted to test different model properties. Tests ranged from mesh sensitivity analysis and hydrostatic test to comparison with other data. These tests were done before the model was incorporated into SIMA.

Mesh Sensitivity Analysis

The initial step involved choosing a coarse mesh size to start with and running a simulation. Following this, the mesh size was halved, and a new set of simulations was performed. This process continued until the results showed convergence. For our project, the convergence criterion was set to 1%.

WADAM's user manual suggests a mesh size of at least 1/6 of the wavelength (DNV, 2017). Based on this approach the minimum mesh size was 1.4 meter, we chose 2 meters as initial condition. Calculations was done according to (*equation 5.1).*

$$\lambda = \frac{g * T^2}{2\pi} \qquad\qquad 5.1$$

$$\frac{f(x)_n - f(x)_{n+1}}{f(x)_n} < 1\% \text{ Criteria is violated} => Mesh\ depenetes \qquad 5.2$$

λ is the wave legnth

T is the periode

Convergence Results

The study led to a final mesh size of 0.5 meters, this satisfied the convergence criteria (1%). It can be seen on the tables that when the mesh size was reduced from 2 meters to 1 meter, the added mass for the surge differed by 3%. However, further reduction to 0.5 m led to a 1% difference. Further reduction resulted in changes between 1% and 0%.

Mesh Size	A11 Surge [Kg]	A22 Sway [Kg]	A33 Heave [Kg]	B33 Heave [Kg]	MESH COUNT
2 [m]	4,96E+06	3,57E+05	4,10E+06	1,69E+06	1,00E+01
1 [m]	4,83E+06	3,52E+05	4,04E+06	1,72E+06	4,00E+01
0.5 [m]	4,78E+06	3,50E+05	4,01E+06	1,72E+06	8,00E+01
0.25 [m]	4,75E+06	3,49E+05	4,00E+06	1,73E+06	1,60E+02

Table 2: Results from mesh convergence study values of added mass is compared

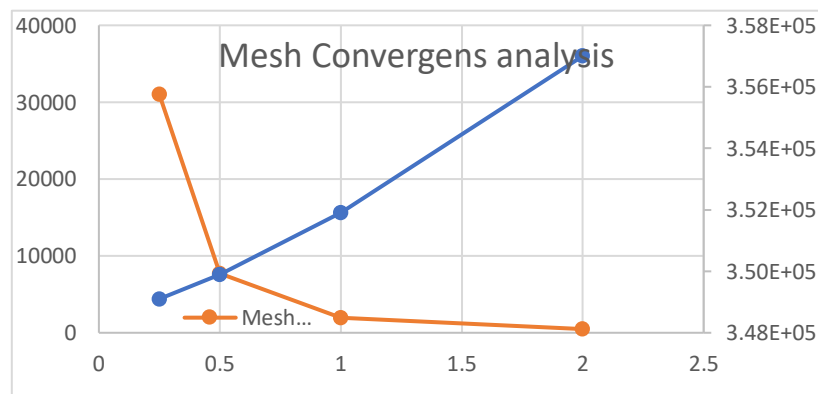| Mesh Size	A11 Surge	A22 Sway	A33 Heave	B33 Heave
2 m - 1 m	1 %	2 %	-2 %	-300 %
1 m - 0.5 m	1 %	1 %	0 %	-100 %
0.5 m - 0.25 m	0 %	0 %	-1 %	-100 %

Table 3: Results from convergence study.

Figure 19: Convergence study

Validation of Hydrodynamic Results by Comparing Values to Independent Study

Model validation is a pivotal step in the model development process, serving to ensure accurate and realistic model outputs. This validation should be conducted before integrating the model into other software or deploying it for results, allowing for the detection and refinement of any flawed models and confirming that the model output aligns with expectations.

In this study, the Wadam model has been validated by comparing the results for added mass and potential damping with results from an independent study. The comparison was made with the results presented in the article "*wave load effects on a long, straight, and side-anchored floating pontoon bridge"* (Dai et al., 2020). The parameters compared included added mass and potential damping for all six degrees of motion: A11, A22, A33, A44, A55, A66, and B11, B22, B33, B44, B55, B66.

To obtain the values, the graphs were measured with a ruler. The graphs were also checked and evaluated to check if they demonstrated similar shape and curvature characteristics. The results of this comparison demonstrated good agreement with the accuracy achievable with a visual inspection. The overall shapes were nearly identical, and the amplitudes looked similar. Values of 4.75 E6 Kg and 4.8 E6 kg were obtained from this model and the independent study. This corresponds to a difference of 1.04 %, which falls within an acceptable range.

This simplified method of validation was chosen based on three criteria's:

1. The time restrictions of this project meant that a comprehensive investigation was not feasible
2. High-quality experimental data was not accessible within the project's timeline
3. The primary aim of this project is to study the impact of a traffic model, rather than the hydrodynamic properties of the pontoons

Validation of mass model by comparison with independent study

By comparing the hydrostatic stiffness of our model with the results presented in "*Appendix A -Global structural model"* and *"static analysis"* (Multiconsult, 2017a), a close agreement was

found. The discrepancy in heave was a mere 1%, which suggests that the hydrodynamic stiffness properties of our model are accurate.

However, significant discrepancies were observed related to the mass inertia properties. For instance, Iyy values showed a difference of 373%, and the discrepancy for Ixx was more than 1000 times. This can be attributed to the use of the 'fill function,' which positioned all the mass at the pontoon's center, including the girder and column mass, in the real world the mass is distributed to the walls of the pontoons.

To compensate for this error, we made some corrections to the mass and inertia of the model in Sima. New values were obtained from table 14.2 of the "Base Case" (Multiconsult, 2017b). The model estimated mass of the pontoon was 912 tons, which included the pontoon mass, sink anodes, and marine growth. Additionally, the inertia coefficient was corrected using data from table 4-10 (p.24) "*Global Structural Model and Static Analysis*" (Multiconsult, 2017a).

Table 4: Updated Mass Inertial

Mass	Ixx [Kgm^2]	Iyy [Kgm^2]	Izz [Kgm^2]
912	2.20E+08	2.30E+07	2.26E+08

Validation of correct Geometry by Checking Volume in GeniE

To validate the GeniE model, we used a straightforward method involving a comparison of the displaced mass. The results calculated from Wadam were compated with the values derived from the "*base case*" at P107(Multiconsult, 2017a). The Wadam values came to 3.354E6 kg, while the table's figures were at 3.421E6 kg. The discrepancy between the two was less than 2%, indicating a relatively low error rate.

This concludes the pontoon chapter, now we will take a look at the structural model

Chapter 6 Structural model
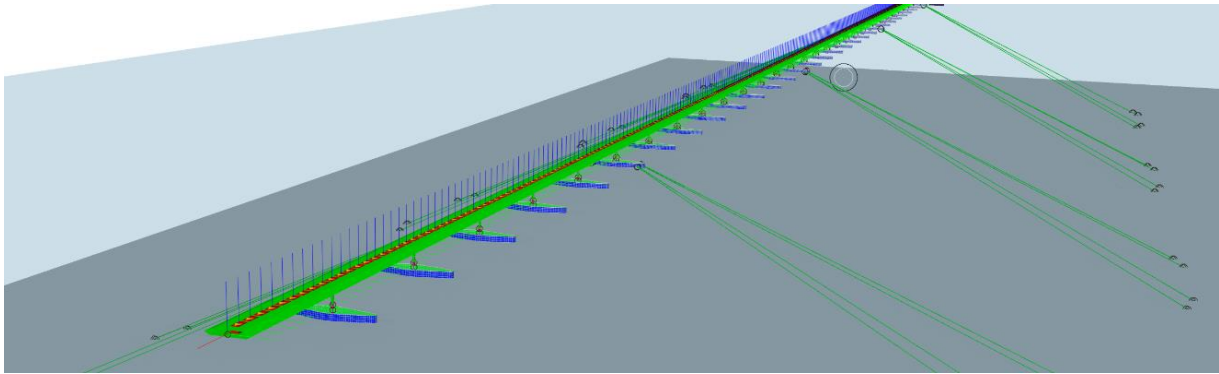
6.1 Intro

This section provides a detailed discussion on the construction of the bridge model. The structural elements are created in RIFLEX, then pontoons are added ass SIMO bodies. The treatment of the traffic model is covered in a separate chapter. The structure of this chapter follows the sequence in which the model was created. The primary steps include the modeling of pontoons in SIMO, followed by a section on the structural model. At the end of each section, brief discussions on validation methods are presented.

Short introduction to software and workbench

SIMA

Version 4.20 of the Simulation of Marine Operations (SIMA) was the main tool for this project. It facilitates time-domain simulations, slender structure modeling, and environmental condition representation. It utilizes hydrodynamic coefficients from HydroD and WADAM, enabling more realistic simulations. For this project, coupled model simulations with RIFLEX and SIMO were employed.

SIMO

SIMO, part of the SESAM package by MARINTEK, simulates pontoon motion in the time-domain. It incorporates the semi-submersible pontoon model and a Morrison model for drag forces. SIMO can model various environmental and hydrodynamic forces and import .SIF files for ease of use with WADAM.

6.2   Defining Global and Local Cordiant system

The first step in the process was to establish the global and local coordinate systems for the model.
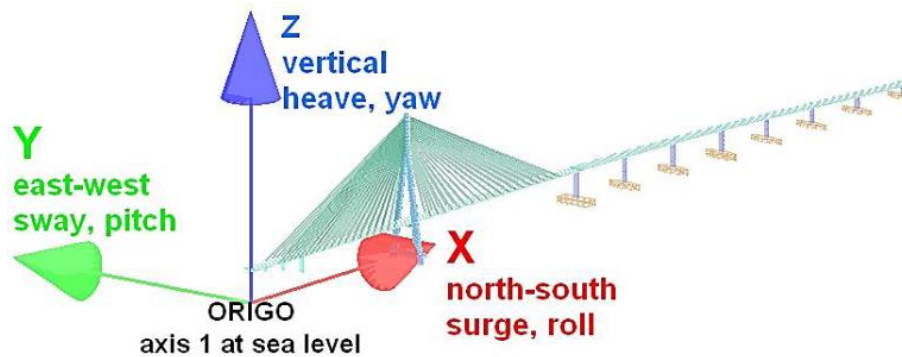
Figure 28: Global coordinate system (Multiconsult, 2017a)

The global coordinate system is the coordinate system used for the structural model, while each pontoon has its own local coordinate system. The global coordinate system is based the one used in *Base Case,* used by Multi Consult, as depicted in (*Figure 28)*. The Z-direction aligned with vertical motion, corresponding to the heave motion. The Y-direction represents transverse bridge motion, which correlates to the sway motion for pontoons. Lastly, the X-direction signifies axial bridge motion, analogous to the surge motion for the pontoons. In the case of the local system, the figure below is illustrating all DOFs.
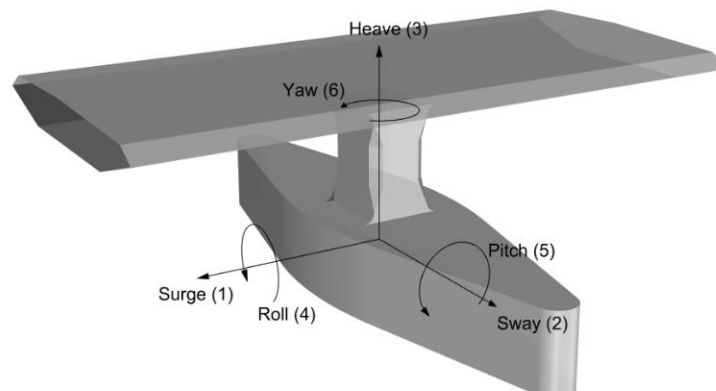
Figure 29: Local coordinate system (Multiconsult, 2017c)

This systematic approach to defining coordinate systems ensures consistency and accuracy across different elements of the model, thereby facilitating more effective simulations and analyses.

6.3 Importing the pontoons as SIMO bodies

The model validation and verification are discussed in a later chapter after the modeling steps.

Next, the pontoons were added, first a set of two pontoons were added to do verification studies on the pontoons. Pontoons were incorporated into SIMA as SIMO 6 DOF (Degrees of Freedom) bodies, using data derived from WADAM (as depicted in Figure 20). The pontoon models were constructed based on structural mass, hydrostatic stiffness, and radiation forces data. Some of these values required adjustments
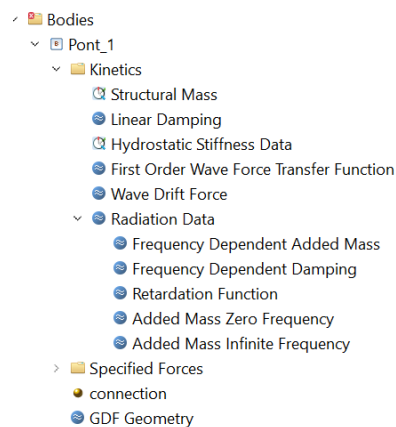
Figure 20: Pontoon data in SIMO

Mass model

When considering a single pontoon, the mass of the model was accurate as it incorporated the full mass of all structural elements. This led to an error when we included other structural elements. The pontoons mass was updated with a new mass based on table values from SSV, this included dry mass and zinc anodes. To validate this new model, a point load were added to the center of the pontoon with a force corresponding to the structural mass. The measured draft where correct.

Hydrostatic reference point

The hydro static reference in heave motion hade to be adjusted with 5 meter in upwards direction
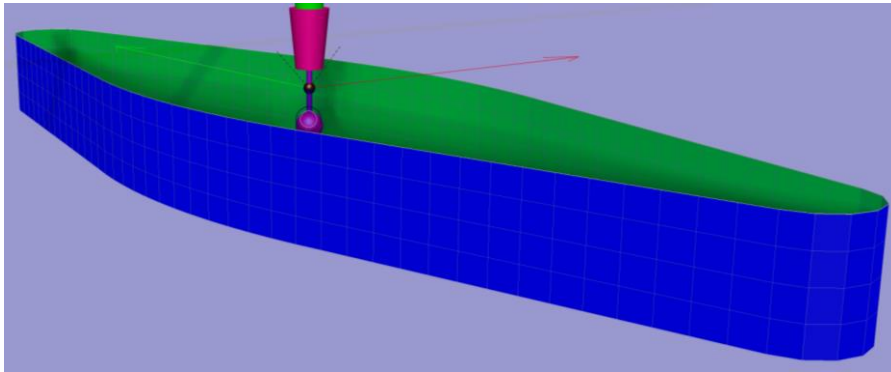

Figure 21: Simo body in SIMA, with simple structure

A connection point was placed at the center of the X-Y plane at the projected water level. This connection point will be used to interface with the structural model, a topic that will be discussed subsequently.

Pontoon spacing

Pontoons are placed with a spacing of 125 meters, this is done according to documentation from SSV.

Validation of model in SIMO

After importing the body containing the hydrodynamic data of the pontoon into SIMO software, the model had to undergo verification to ensure the properties obtained from the WADAM analysis were accurately transferred to SIMO and that the simulations were realistic before coupling with structural elements. The validation process consisted of several tests, comparisons, and evaluations to confirm that all the desired pontoon properties were simulated well. Validation of hydrodynamical stiffness obtained from WADAM

163   Validation of hydrostatic stiffness

The first test involved the validation of the hydrodynamical stiffness obtained from WADAM 6.7013 E3 KN/m this value is found in the stiffness matrix *(Figure 22)*. This was done by comparing the stiffness matrix with an independent study. The hydrostatic stiffness for the pontoons was compared to results found in "*Base Case*" 6.7 E3 KN/m and the values were found to be very close to each other, thereby validating the data (Multiconsult, 2017b).

	x	y	z	rx	ry	rz
x	0.0	0.0	0.0	0.0	0.0	0.0
y	0.0	0.0	0.0	0.0	0.0	0.0
z	0.0	0.0	6.7013e+06	0.0	0.0	0.0
rx	0.0	0.0	0.0	1.465e+09	0.0	0.0
ry	0.0	0.0	0.0	0.0	8.8983e+07	0.0
rz	0.0	0.0	0.0	0.0	0.0	0.0

Figure 22: Pontoon stiffness matrix in SIMO

Validation of mass and draft

The second test involved validation of the draft when adding external loading, such as a bridge girder. The model mass had to be reduced and updated with a new value of 8.5 E5 Tons. When the model was created in WADAM, the draft was set manually to 5 meters, and the mass of the pontoon was calculated based on the displaced volume using the "Fill Function". The calculated mass represents the sum of the mass of all structural elements including the pontoons. This simplification was necessary to obtain the correct hydrodynamical data. The solution was to update the mass model in SIMO, the new updated mass included self-weight, ballast, Zink anodes, and marine growth but exuding structural elements such as columns, and girder. The calculated mass was 912 Tons, this number was based on SSV documentation. However, to get a more appropriate draft the final value where set to 815 Tons.

Table 5: Pontoon mass values, taken from (SSV)

Steel	Pontoon mass [Ton]	Zink Anode [Ton]	Marine growth [Ton]	Total Mass [Ton]
Axis 26	*809*	37	66	912

Validation of added mass

The third validation compared the imported values for added mass and potential damping with recalculated values from SIMO. This was done according to recommended procedure found in SIMA manuals: "Compare and re-calculate retardation function". The check was based on comparing values from WADAM, with re calculated values from SIMO. Results showed grate agreement, validating the WADAM results and the data transfer (DNV).
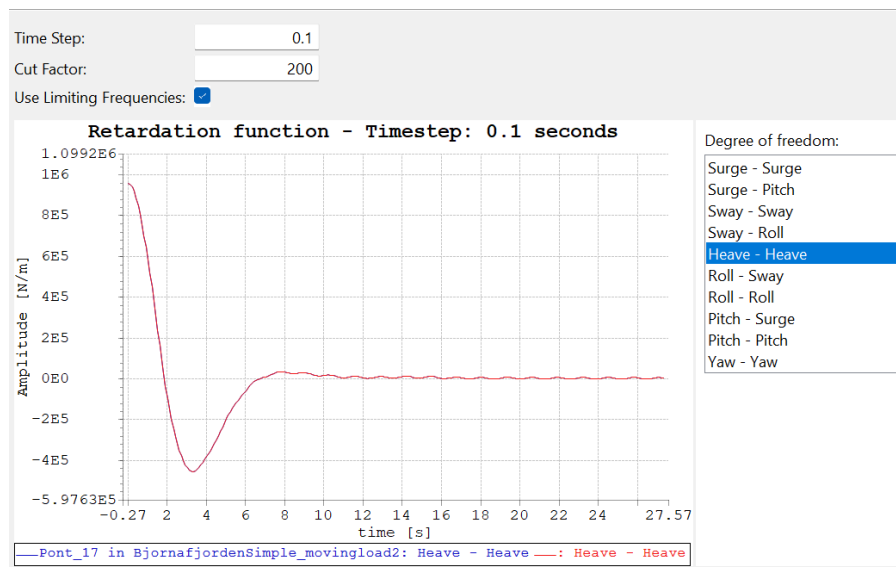

Figure 23: Heave motion, calculated in WADAM and Simo

Validating wave response

The final step in the validation process for the pontoons involved conducting a wave response simulation with various regular wave conditions. Three scenarios simulated were: short waves, waves near the natural frequency, and long waves. The purpose was to ensure that the model was accurately simulated under different conditions. To maintain the pontoons' position, horizontal stiffness was incorporated. Wave periods of 1 second, 10 seconds, and 100 seconds were utilized.

In the short-wave simulation, the pontoons remained steady, with only minor movements observed. This represents the inertia domain, where inertial forces dominate. When waves had the same period as the eigenvalue in heave motion, vertical oscillations increased with time, signaling a resonance effect. The amplitude flattened when reaching a certain height, indicative of the damping domain where damping forces are dominant. The final domain was the one

influenced by hydrostatic stiffness. In this situation, the pontoons moved with the wave, maintaining a similar amplitude.

The verification process was instrumental in affirming the accuracy of the hydrodynamic model generated in WADAM, resulting in realistic simulations and forming a solid foundation for coupling with the structural model. The conducted tests, comparisons, and evaluations offered valuable insights into the precision of the outcomes and fostered confidence in the model's reliability.

6.4   Structural modeling in RIFLEX

Intro to structural modeling

Modeling of the bridge structure was done in Riflex. This section is intended to give the reader an overview of the overall prosses around modeling. After the structural model where created, a coupling prosses was done to link the models.

Software: Riflex

RIFLEX is an advanced tool developed by MARINTEK to model riser systems and slender bodies. It is a part of the Deep C package within the SESAM. It is run from the SIMA workbench. The tool is designed for both static and dynamic analyses.

The software was selected based on its capabilities in analyzing slender structures. The floating bridge is a long slender structure for which RIFLEX was well-suited for analysis. Additionally, the software can handle large deflections and small bending stiffness. It can handle both static equilibrium problems and dynamic analysis, including calculations of eigenvalues. In addition it is capable of handling responses to both regular and irregular waves. Therefore, RIFLEX was chosen as the software to conduct the structural modeling and analysis.

RIFLEX comprises of five modules that communicate with each other to solve tasks. These modules have different purposes. The INPMOD module is where data is inputted and organized. The STAMOD module performs different types of static analysis, with the results used as input for the DYNMOD module, which handles dynamic simulations. Furthermore, the OUTMOD module handles the post-processing of selected data from STAMOD and DYNMOD. The file communication system is illustrated below (Ocean, 2017).
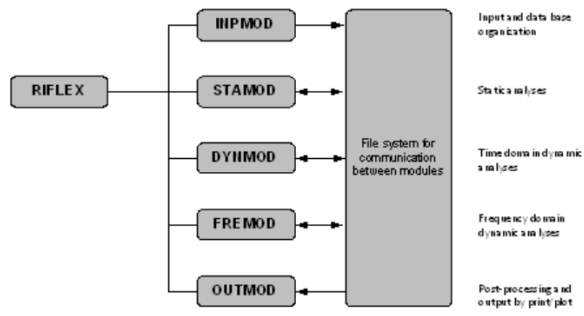
Figure 24: RIFLEX file communication system, taken from RILEX user manual, ch 1.3 (Ocean, 2017)

Modelling

To construct the model, a specific sequence of steps is followed. It starts with creating super nodes which act as connection and attachment points. They will also form the foundation for the line connections. Subsequently, lines are connected between nodes and overlaid with a cross section. The pontoons are connected to the model via columns. Mooring lines are attached to the pontons vi attachment points. To incorporate traffic loads, model alterations are required, which will be detailed in the next chapter. A discussion on the slender system will be presented in the following section.

Defining a Slender System

To create the structural model a slender system task was initiated (*Figure 25*). This task includes data on lines, line types, cross sections, and supernodes. All these topics are elaborated on in the following section. The pontoons model is stored as a SIMO "Bodies". Pontoon models are coupled with the slender system, this prosses is discussed later.
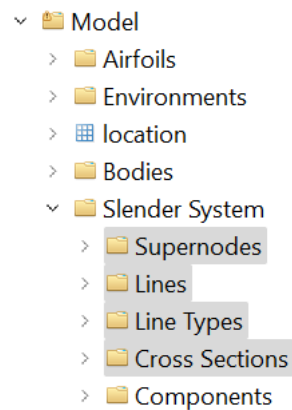
Figure 25: SIMA TASK: slender system and Simo bodies

Supernodes
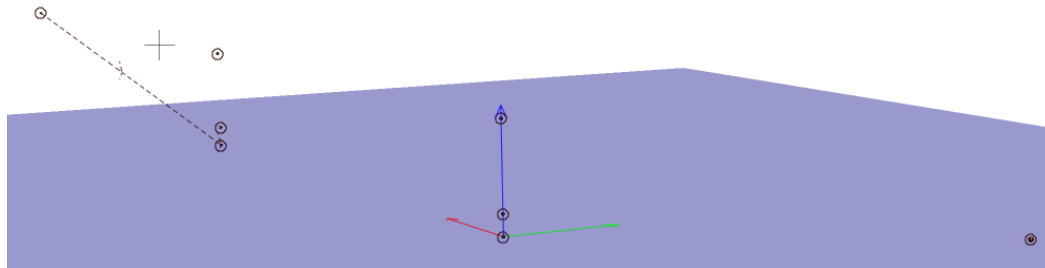
Figure 26: S-nodes, B-nodes, and P-nodes in SIMA

Riflex utilizes super nodes as connection points between various structural elements, such as pontoons, girders, and columns. Each node are placed with in the cartesian coordinate system, then a a boundary condition is assigned. On (*Figure 27*) you can see a simplified illustration of the node arrangement, ass well as a cross-section of the deck, column, and pontoon. Nodes 1 and 4 is connectin the bridge girder sections together and are named B-node. They are placed at an interval of 125 meters with a height of 18 meters. These nodes are assigned **free** boundary conditions, except the end nodes, which are treated in the next section. Below each B-node there are two nodes. Surface node (SNode) and pontoon node (PNode). The S-nodes are located on the water surface and is assigned **free** boundary condition. The P-nodes are placed at a height of 3.5 meters, representing free board height. These nodes are assigned with a **slave node** boundary condition. Slave nodes follow the movement of the master nodes. The master nodes are discussed later.
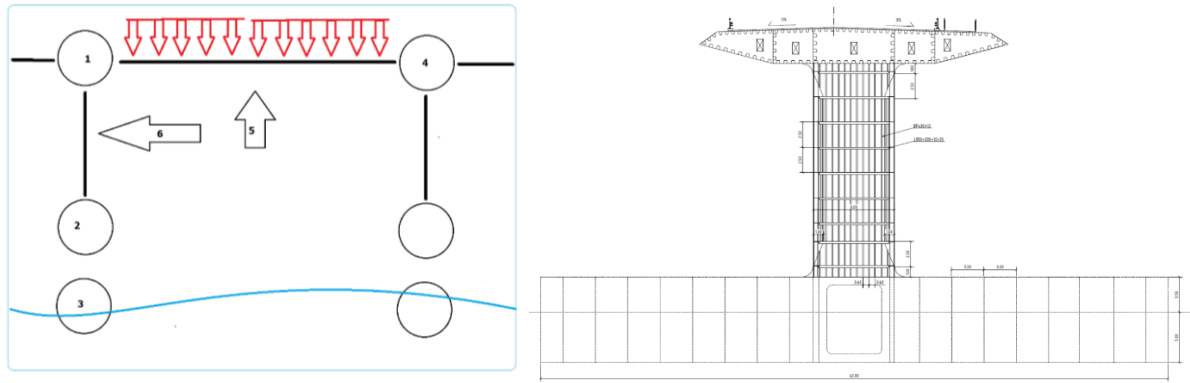
Figure 27: Illustration of node placement, and structural elements.

Modeling of Bridge Girder and Cross-Section
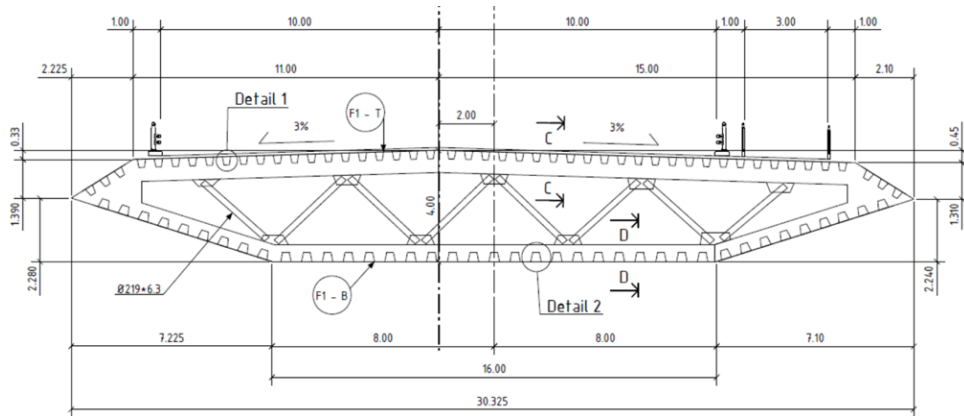
Figure 28: Cross-section (SSV, Multiconsult)

Girder Analysis

The structural function of the girder is to carry the traffic and transfer the loads from the spans to the columns. Various cross sections have been designed to accommodate different sections such as the cable-stayed sections and the floating bridge sections. The deck is angled at 15 degrees to enhance aerodynamic performance. Additionally, the girder incorporates stiffeners to boost its bending stiffness, with both transverse and throughout stiffeners employed.

Transverse stiffeners are placed at 4-meter intervals. The steel type S420N is used. The project-relevant data is presented in the table below. An illustration that indicates what type of sections is used for the different sections is also presented.
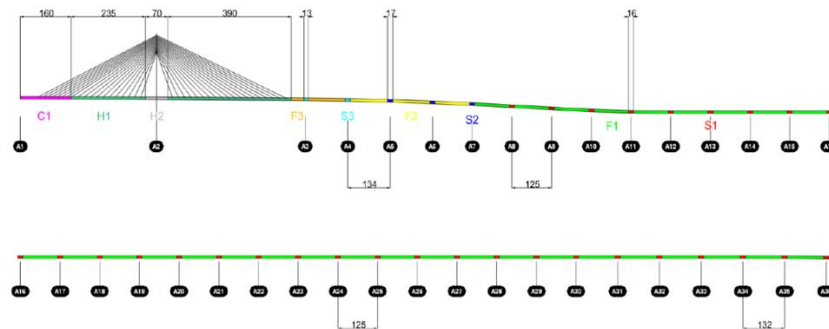
Figure 29: Illustration relating the different cross sections to the bridge section.

According to the SSV tables, six different cross-section variants have been employed for the low bridge. There are three types of field sections defining the spans: F1, F2, and F3 and there are three types of support sections S1, S2, S3 which are used at the interconnection between column and girder.

Model choice

Because of time restrictions and the purpose of the study, only one cross-section was included. Relevant data is presented in the table below.

F1 Cross - section properties	
Section Name	F1
Material	S355-S460
Sectional Area (m2)	1,5E+00
Mass Coefficient (Kg/m)	16 000
Axial Stiffness E.A. (N/M)	2,40E+11
Bending stiffness Weak axis Y E.I. (KN*m2)	6,67E+11
Bending stiffness Strong axis Y E.I. (KN*m2)	1,88E+13
Torsion Stiffness (KNm2)	5,37E+11
Radius of Gyration (m)	8,3

Column Analysis

The function of the column is to transfer the horizontal and vertical forces from the bridge girder to the pontoons. This is done with rectangular hollow steel tubes. A chamfer is applied to the corners to improve aerodynamics. A steel bracket made of S420N is used between the girder and column to reduce stresses.

Figure 30: Illustration of column, taken from "Base Case" P. 94

In the analysis, three different types of columns were found. To simplify the modeling all columns where modeled with the same dimension. Relevant data is located below.

Column dimensions	
Axis	12 - 27
Material	S355-S460
Height [m]	8
Width [m]	6
Thickness [mm]	40
Height [m]	10,5
Weight [Kg/m]	11994
Ix [m4]	12,94
Iy [m4]	14,92
Iz [m4]	9,65

Tabell 1 Tabell 2: Cross - sections properties for columns, taken from "Base Case" P.93

Lines and line types

In the model, spans and columns are modeled with lines. These lines were established between the supernodes. Each line is defined by a line type, which encompasses length, element number, and cross-section data. Two principal line types were developed: one for the bridge span and another for the columns. Below is a figure visualizing the lines (green tubes).
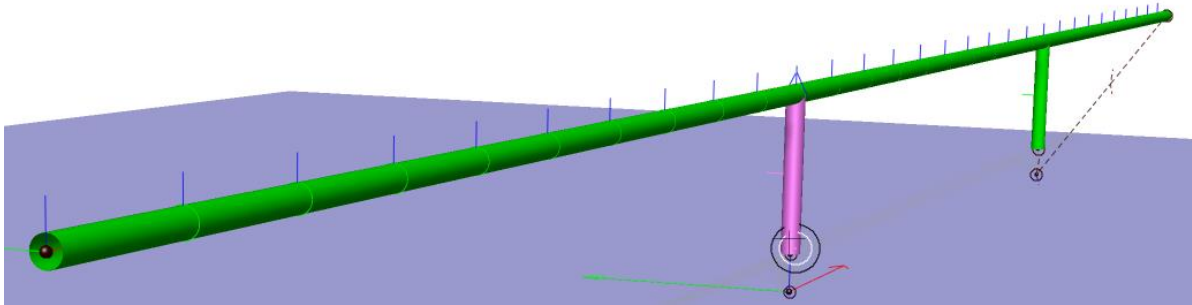
Figure 31: Lines representing spans, and columns are added

Boundary conditions

Boundary conditions were applied to the end nodes, named *end1* and *end2*. All degrees of freedom were **fixed** at both nodes, this is illustrated on the figure below.

Figure 32: Settings for END1

Linking pontoons and slender system

A connection-node was created in the center of the SIMO bodies. This node was connected to the S-node at the corresponding location. No artificial stiffness was introduced. In addition, a panel model was added to each pontoon for the purpose of visualization. A model section

containing three pontoons is illustrated below. You can see the connection node in the pontoon center.
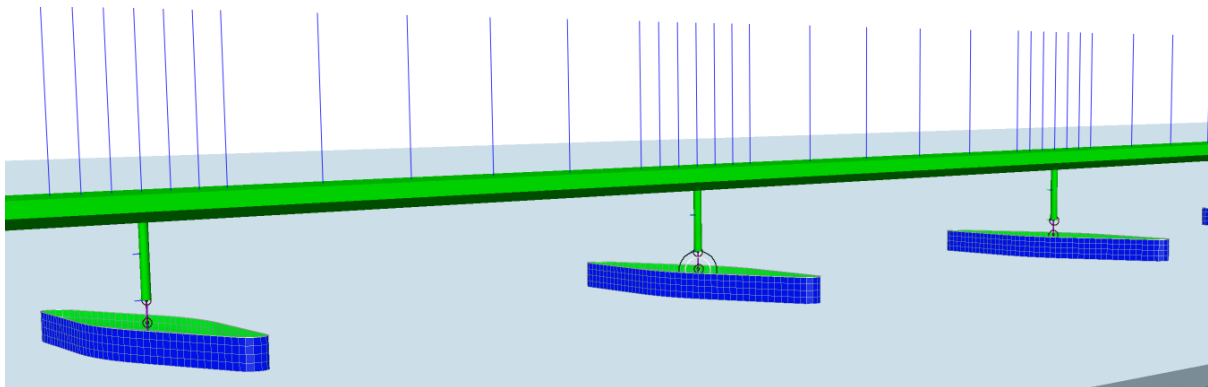
Figure 33: Section of the pontoon and bridge model

Moring lines

Morin lines were attached to points on the pontons and the. Data on locations is presented in documentation from SSV (vegvesen, 18). A total of 8 mooring lines were used for each pontoon. Lines were modeled as a linear bar element. In addition, and Morrison model was added for improved drag simulation.
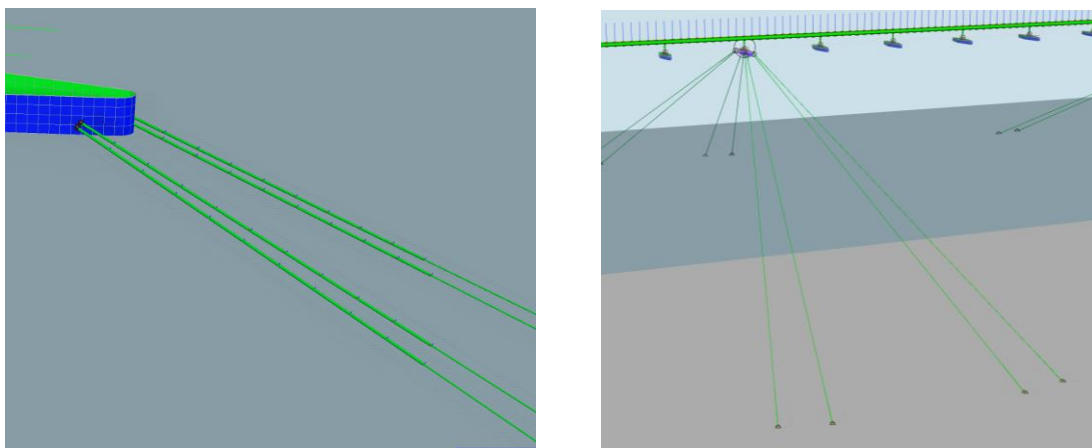
Figure 34: Illustration of moored pontoon

The full bridge model was created with these elements. Only the lowewer section is modeled, excluding the cable stay section. This was done to simplify the model and remove unnecessary elements. Super nodes and pontoons are placed according to *tabel 4-1*, *page 13 A App A*

(vegvesen, 18). In the following section, some illustrations of the coupled model is presented, followed by a section on model validation. The bridge discretization and traffic modeling are discussed in the following chapter.
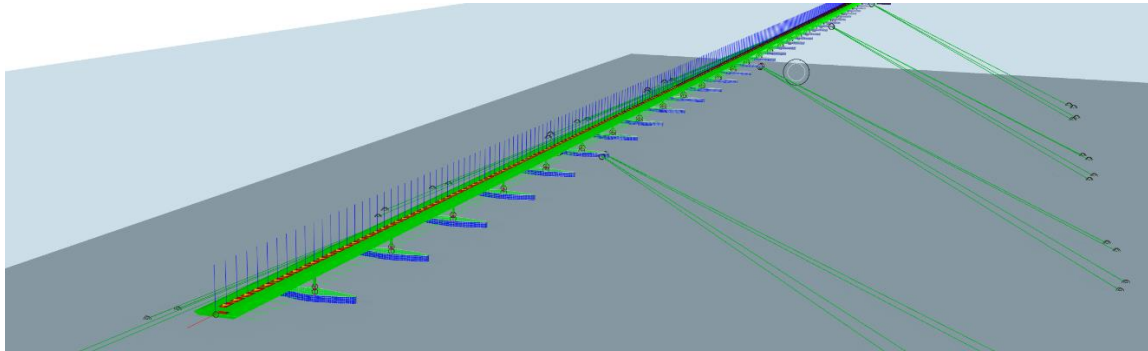
Figure 35: Isometric view of the bridge
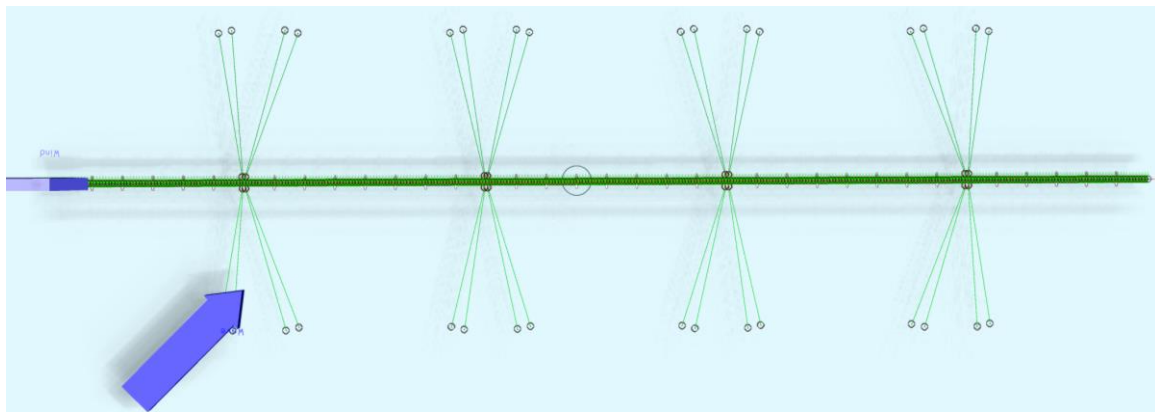
Figure 36: Top view of the bridge
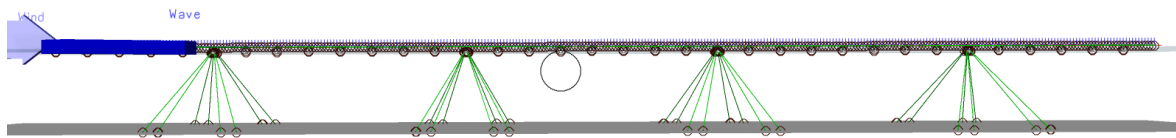
Figure 37: Side view of the bridge

6.5   Validation: Comparing results with an analytic solution

Validation of the structural model involved a static load test without traffic. The test was intended to check if the vertical deflection of the girder were coherent with alternative methods. As the floating bridge is one of its kind, some simplifications had to be done to generalize the problem.

The model was simplified to a single span beam with a **fixed–fixed** boundary condition. Only dead loads are considered. An illustration of the problem is presented bellow (Figure 38). The second method involved manual calculations done in Excel based on the Euler – Beam Theory. Equations are presented in chapter 3.
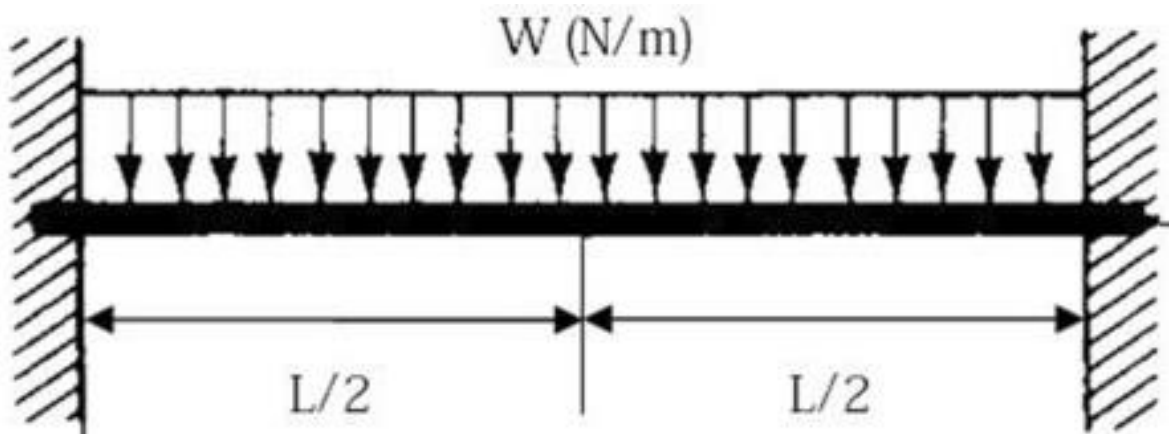
Figure 38: Beam fixed at both ends with the distributed load.

Results

It can be seen from the results presented in the table below that values where in the same range. The biggest difference was 0.33 mm. This validates the model

Static analysis and analytic solution for single span			
Riflex Position [m]	Riflex Deflection [mm]	Analytic Deflection [mm]	Error [%]
18.00	0.0	0.0	0
17.99	9.0	9.5	-5
17.97	33.0	33.0	0
17.94	64.0	64.0	0
17.90	97.0	97.0	0
17.87	127.0	127.4	0
17.85	151.0	151.7	0
17.83	166.0	167.3	-1
17.83	171.0	172.8	-1
17.84	165.0	167.6	-2
17.85	149.0	152.2	-2
17.88	124.0	128.1	-3
17.91	93.0	97.8	-5
17.94	60.0	64.9	-8
17.97	28.0	33.7	-20
18.00	4.0	9.9	-148
18.01	-6.00	0.00	100

Table 6: Results from static analysis and analytic solution

*Maximum deviation 0.33 mm

Based on this validation program, the structural model is simulating well, and results are good. In the next chapter, a discussion on the traffic simulation, bridge discretization and validation of dynamic behavior is presented

Chapter 7 Preparing the structural model for traffic loading

7.1 Intro

In this chapter, a discussion around the implementation of traffic loads is discussed. This includes topics like discretization of the bridge and traffic model as well as simulation data. This chapter begins with the steps of discretization, then move on to validation ending with a section discussing the simulations parameter.

7.2 Discretizing the bridge girder to create loading points

The girder was discretized into smaller segments to make it possible for dynamic loading to take place. Each span was divided into 10 segments consisting of 11 nodes. Three nodes can be seen on the left illustration (Figure 39). **SIMO bodies** were added to each node. This bodies could handle external force files. Each body got a **6 DOF** condition and where connected to the slender system via the nodes. The bodies can be seen as the red boxes. Then a set of new shorter line segments were added. In addition, a cross-section model was added for visualization properties.
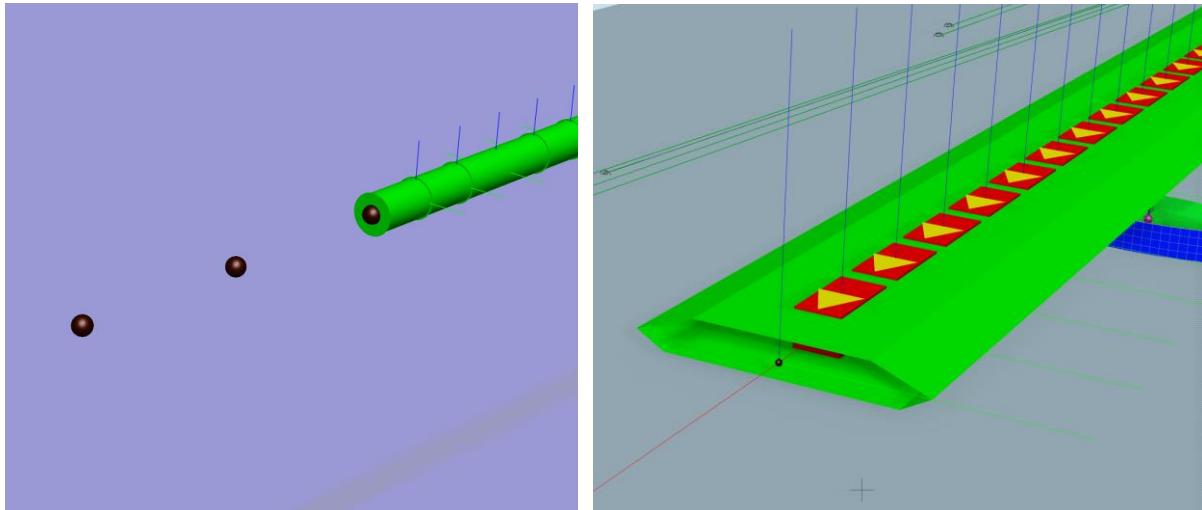
Figure 39: New B-nodes, line segments, and bodies.

External force-file

SIMO allows for user-defined input files. This function is used to simulate the traffic loads. Each SIMO body (girder) is assigned its own load sequence via a force file generated with a MATLAB code. The force file consists of a 6-column matrix with numerical values

representing the loads from the traveling vehicle in Kilonewtons. In this project, only forces in the Z direction (column 3) are included. For each traffic condition and individual file must be uploaded.
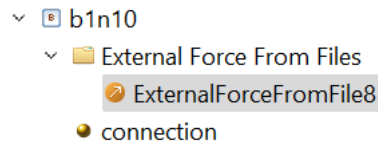

Figure 40: External force file, located at the girder bodies (red boxed)

Traffic simulation

In this section, a brief discussion on traffic generation and data handling is presented. For a more detailed explanation, please visit Chapter 3. Traffic data is generated with a Python code and exported to an Excel sheet with the file extension (.CSV). Data includes position, time, and vehicle type. A MATLAB code, provided by the supervisor Jian Dai, adds a force vector to the moving points, this vector can be manually adjusted to change the magnitude. This gives the opportunity to simulate different types of vehicles.

Subsequently, a third script is handling the discretizing the time and position dependent loads into separate files for each node. A visual representation of the generated traffic data can be seen in *(Figure 41)*, which shows both trucks and cars. After some post-processing, the data will resemble the format shown in (Figure 42). This data is imported to SIMA.
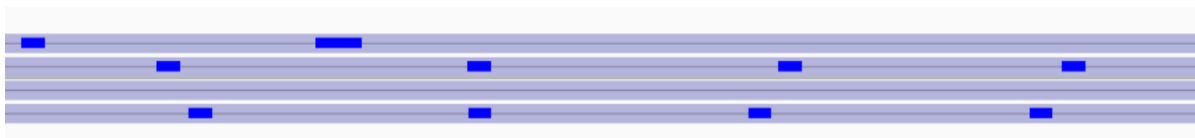
Figure 41: Traffic flow visualized. Four lanes, trucks and cars can be seen

```
0 0 0 0 0 0
0 0 0 0 0 0
0 0 -1.783066e-01 0 0 0
0 0 -2.370724e+00 0 0 0
0 0 -5.783662e+00 0 0 0
0 0 -8.789760e+00 0 0 0
0 0 -9.764168e+00 0 0 0
0 0 -7.933386e+00 0 0 0
0 0 -4.610857e+00 0 0 0
0 0 -1.423941e+00 0 0 0
0 0 0 0 0 0
0 0 0 0 0 0
```

Figure 42: Section of external load file. The third column is loaded in the vertical direction in kN. The sequence represents a car at 1 ton passing at 110 km/h

7.3   Validation of structural dynamics and traffic model

A validation study was conducted to test the structural behavior in response to traffic. This test will focus on the dynamic response of the bridge. The static response has already been validated.

The objective was to evaluate if the response to moving loads was in line with alternative methods. The focus is on vertical displacement and eigenvalues. This was achieved by comparing with an analytic solution discussed in Yang's paper, which describes the deflection of a curved beam subjected to moving loads (Yang & Wu, 2000).

Simplifications and Assumptions

In the paper, they use a single span beam with **pin-pin** supports illustrated on *(Figure 43)*. To address this a simplified model were created with similar boundary conditions, comprising of a bridge section made of 10 segments pinned at both ends, the model is illustrated below *(Figure 44)*.
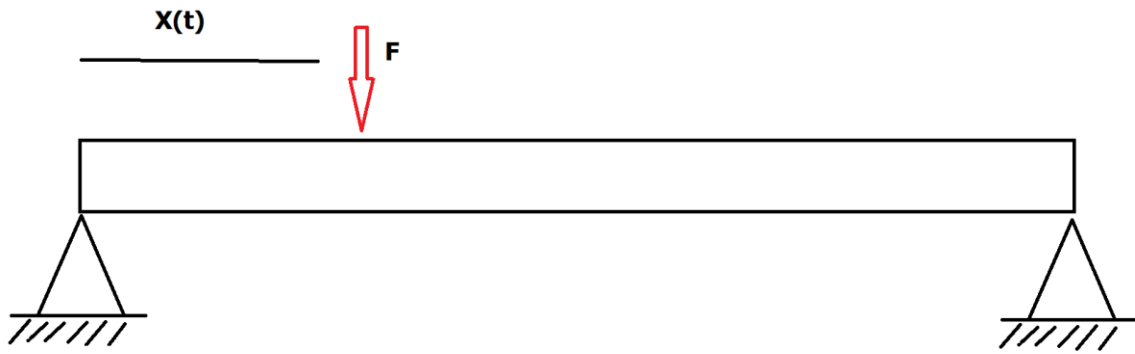
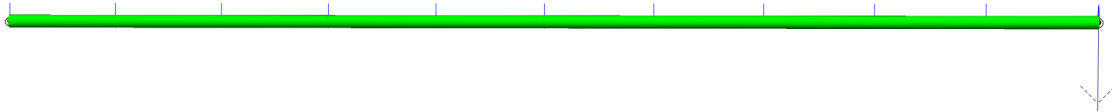Figure 43 Moving load on beam with Pin-Pin support

Figure 44: Model made in Riflex with Pin-Pin boundary connection

Results

Results from the deflection analysis showed poor agreement. The vertical displacement was off more than 1000 times. To address this a new study was done with new vehicle parameters. The vehicle speed was set to 1m/s. Results were similar. To find the error a comparison was made with a static load test. This test was based on the Euler beam formulation. This test indicated that the Riflex model where correct. Result from the eigen value analysis demonstrated relatively good agreement, with a discrepancy of only 7% between the two sets of results.

A difference of 0.7% indicated that the Riflex model is simulating appropriately.

MODES

The first mode was investigated and compared with the vibration response. In (Figure 45), you can see the first mode, which corresponds to a period of 1.44 seconds. By measuring the period of the oscillations induced by the moving load, we determined that the first mode was excited. The measured period was 1.55 seconds. A difference of 0.7% indicated that the Riflex model is simulating appropriately.
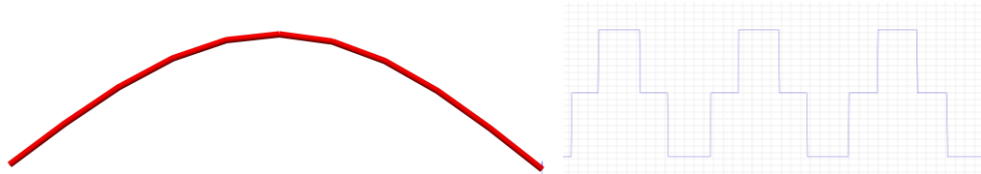

Figure 45: Mode shape 1, period 1.55 s

Comparison of Vertical Displacement from Riflex with Analytic Results

Deflection values obtained from Riflex were compared with those obtained from a static solution. where the speed was set to 1 m/s. The results presented on *(Figure 46)* show good agreement between both methods. The numerical method predicted 1.55 millimeters and the analytic solution predicted 1.775 millimeters. This result indicates that the model simulates properly with respect to vertical deflection. Below is a figure representing the results from Riflex
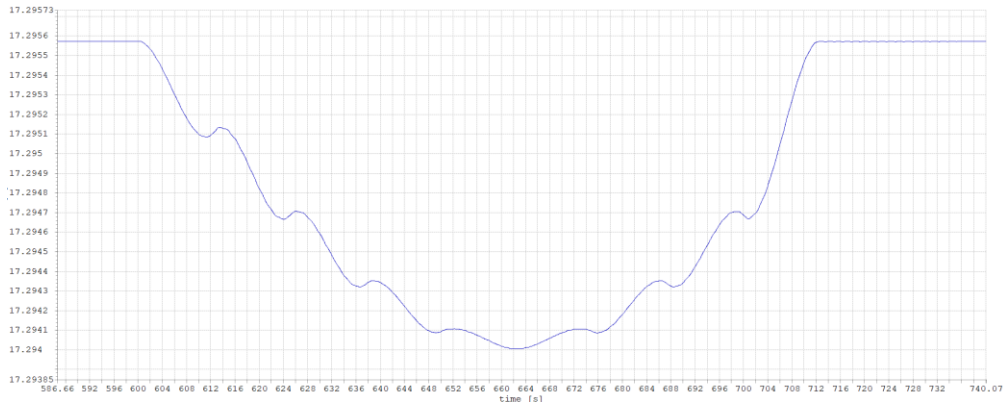
Figure 46: Response to moving load (1m/s, 3000kg).

7.4   Simulation Parameters; Traffic conditions & Environmental loads

To examine the vertical response of the bridge, several simulations under varying conditions were carried out. The experiments can be divided into two categories. The first is the parametric study, where different vehicle parameters such as mass and speed were tested to gain a better understanding of their influence on vertical deflection. The second is a stochastic analysis of typical traffic scenarios , with and without waves. This is designed to identify the conditions that result in the greatest deformations. In the following sections, the simulation parameters are presented, starting with the parametric study.

Parametric Study to Determine the Effect Mass & Speed

The first simulation was conducted to study the relationship between mass and vertical motion. Motion is measured at the pontoon center and bridge nodes. Since the focus of this study is on the vehicle parameters, waves are simulated with a height of 1 cm representing a calm sea. The simulation time is set to 500 seconds, which is sufficient to allow traffic to build up and cross the bridge from both directions. The vehicle flow rate was set to 1 vehicle per minute per lane; this number is low and well below the free-flow condition. Wind and current are neglected. In the following two sections, specific details regarding each simulation are presented.

Effect of Changes in Mass

In this experiment, three simulations were simulated. For each simulation, the mass was altered. A mass of 1 ton was chosen to represent a typical car, a mass of 25 tons to represent a medium-sized lorry, and a mass of 50 tons to signify heavy traffic, such as a trailer loaded with timber. The speed was set to 110 km/h; this is not realistic for heavy vehicles, but it does not interfere with the objectives of this study. All parameters are detailed in the (*Table 7*). Additionally, a figure is provided on the following page to illustrate the load sequence for the 1-ton load case. Some peaks are visible at 20 kN. These occur as two vehicles pass the same node in opposite directions, as illustrated in (*Figure 47*).
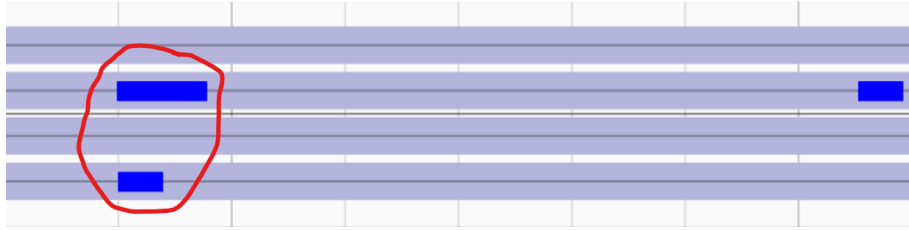
Figure 47: Two vehicles passing the same node at the same time

- The traffic model does not provide options for selecting individual types of vehicles, such as cars or trucks. This issue was solved by equalizing the masses of trucks and cars, thereby allowing for joint adjustments.

PARAMETRIC STUDIES: EFFECT OF VEHICLE-MASS				
Sim Nr	UNITS	1	2	3
Wave Con	[-]	Calm	Calm	Calm
Amplitude	[m]	0.1	0.1	0.1
Period	[S]	4	4	4
Veh Type	[-]	Mix	Mix	Mix
Speed	[km/h]	110	110	110
Traffic Rate	[v/min/ln]	1	1	1
Share of Truck	[%]	20	20	20
Mass	[Ton]	1	25	50
Time	[S]	500	500	500

Table 7: Vehicle parameters used in mass study
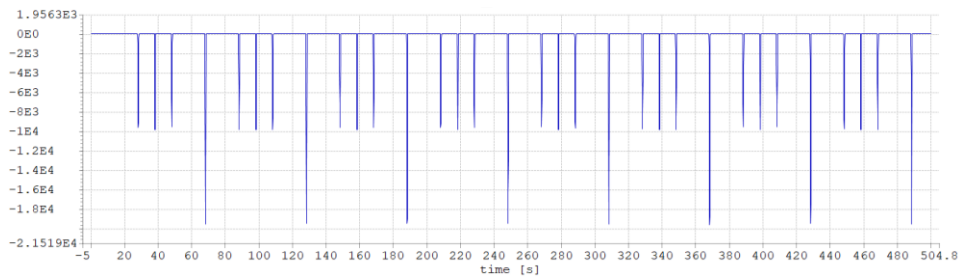
Figure 48: Load sequence for vehicle at 1 ton used for node B2N2

Effect of Changes in Speed

These simulations were conducted to study the impact that changes in velocity have on vertical motion. As a vehicle's speed influences the cyclic loading frequency, it could provide valuable insight. Many of the parameters are similar to those in the mass effect simulation, but there are two main differences. Now, two different masses are simulated. Cars are modeled with a mass of 1 ton, and trucks are modeled with a mass of 25 tons. Two simulations were conducted at speeds of 55 km/h and 110 km/h. An illustration of the load sequence is presented below, and the general data used is provided in the table below (*Table 8*).

PARAMETERIC STUDIE: EFFECT OF VEHICLE-SPEED				
Simulation Nr	**UNIT**	**1**	**2**	**3**
Wave Con	[-]	Calm	Calm	Calm
Amplitude	[m]	0.1	0.1	0.1
Period	[S]	4	4	4
Type	[-]	Mix	Mix	Mix
Speed	[km/h]	0	55	110
Flowrate	[v/min]	1	1	1
Truck rate	[%]	20	20	20
Mass	[Ton]	1 & 25	1 & 25	1 & 25
Time	[S]	500	500	500

Table 8: Table contain data for speed simulations
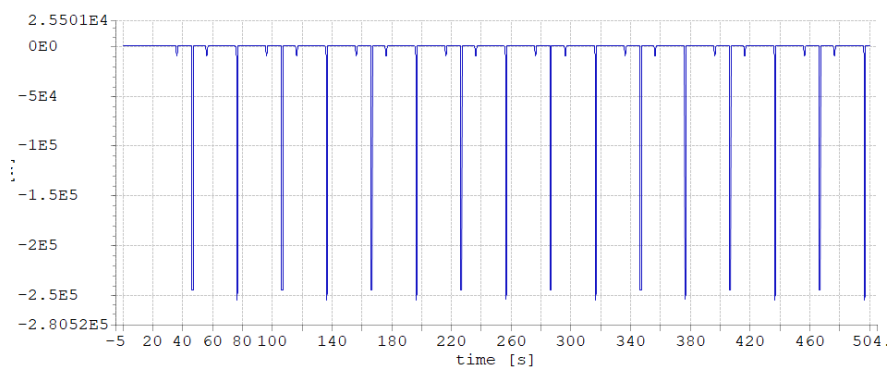
Figure 49: Load sequence for 55 km/h speed test

7.5 Stochastic Study: Traffic Conditions

Both traffic and environmental loads are intrinsically random. To account for this, a stochastic analysis was implemented. Each simulation was run for 1 hour. Originally it was intended to simulate three hours, but this was not feasible as the data was too large for Excel to handle the congested state (to many data points). In total, four simulations were conducted for three different traffic conditions. Additionally, a simulation was conducted without waves for comparison. Relevant data is displayed in the. Car following parameters are assumed to be similar for all conditions (*Table 9*).

```
#car following parameters
T_passengerC=1.5
T_truck=2.0
v_max_passengerVeh=30##Max Speed
v_max_Truck=25##Max Speed
s0_passengerVeh=2
s0_Truck=4
a_max_PC=1.4
a_max_Truck=0.7
```

Table 9: Car following parameters

Free traffic flow

Free traffic flow refers to a condition where the volume of traffic is low, enabling each individual vehicle to travel at its desired speed. There is minimal interaction between vehicles. This state is typical for late-night or early morning hours. An illustration is provided below (*Figure 50*). For this project, the flow rate is assumed to be 2,400 vehicles per hour, each traveling at an unrestricted speed.

Figure 50: Free flow traffic (2,400 veh/hour)

Capacity

Capacity refers to a state where the maximum number of vehicles that a road can accommodate without causing disruption is reached. It is quantified in terms of volume, taking into account various conditions such as speed limit, weather, and vehicle type. An illustration of this condition is provided below *(Figure 51)*.. The volume flow in this scenario is 9,600 vehicles per hour, and vehicles are traveling at an unrestricted speed.
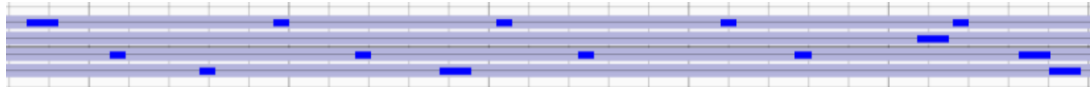

Figure 51: Capacity (9,600 veh/hour)

Congestion

Traffic congestion refers to a situation where the volume of traffic exceeds the road's capacity, consequently reducing speeds and increasing vehicle interactions. Congestion can potentially lead to traffic jams. An illustration of this condition is provided below *(Figure 52)*. For this project, the vehicle speed is reduced to 36 km/h, resulting in a traffic volume of 38,400 vehicles per hour.

Figure 52: Congestion (38,400 veh/hour)

No-Wave

This simulation mirrors the free traffic flow condition, with one key difference being the environment. In these simulations, the waves are considered calm. This simulation was conducted to assess the impact of traffic in comparison to that of waves.

	Unit	FREE	CAPAC	CONGEST	NOWAVE
STOCHASTIC STUDY: EFFECT OF DIFFERENT TRAFFIC CONDITIONS					
Waves	WAVE	WAVES	WAVES	WAVES	Calm
Amplitude	[m]	1.6	1.6	1.6	0.1
Period	[S]	5.3	5.3	5.3	4
Type	[-]	COMB	COMB	COMB	COMB
Speed	[km/h]	110/90	110/90	110/90	110/90
Flowrate	[v/min]	2,400	9,600	38,400	2,400
Truck rate	[%]	20	20	20	20
Mass	[Ton]	1 & 25	1 & 25	1 & 25	1 & 25
Time	[S]	10800	3600	3600	3600

Table 10: Stochastic study parameters

Environmental Loads

Waves were modeled as irregular waves heading from one side. For this project, we utilized wind waves with a 1-year return period based on a study done by SSV (SSV, 2018). The waves are modeled using the Jonswap spectrum with three parameters. The wave height is 1.6 meters with a period of 5.3 seconds. The waves' direction aligns with the Y-coordinate axis. Relevant data can be found in (*Table 11*). Both current and wind have been neglected.

	UNIT	SLS 1Y	Calm
ENVIRONMENTAL PARAMETERS: WIND WAVES 1Y RETURN PERIOD			
HEIGHT Hs	[m]	1.6	0.1
PERIOD Tp	[s]	5.3	4
DIRECTION	[deg]	90	90

Table 11: Environmental data for wind waves

Chapter 8 Results

8.1 Global and Local Structural Response

In the subsequent section, the structural response is analyzed when subjected to various traffic and environmental conditions. This section is divided into two subsections, each handling different results. The first subsection entails an analysis of the parametric study on vehicle mass and traffic speed, with waves assumed to be calm. Following this is a section analyzing the results from the stochastic analysis, which includes waves and different traffic conditions.

Values are extracted from nodes, bodies, and elements. Pontoon response values are derived from the SIMO bodies, the girder displacement is taken from the beam nodes, and the moments are measured from the line segments (left side). Two main types of plots are utilized. The first type encompasses all data and creates a plot with maximum or mean values for all locations to facilitate a better understanding of the global response. The second type of plot illustrates motion or moment as a function of time for a localized area (nodes or elements).

8.2 Parametric Study of Vehicle properties

Vertical Motion for Different Loads

The figures below present the results of vertical displacements when the vehicle mass is set to 1, 25, and 50 tons. These figures capture the overall response. The section from A1-A6 is not considered as this section possesses different stiffness properties. Motion is larger in the 5 pontoons located between the moored one's pontoons example A8-A12. The moored pontoons (A6, A14, A22, A30) exhibit much less movement than the unmoored pontoons, although there are exceptions. The pontoon pair surrounding the moored pontoons shows even less motion, A5 and A7. Another observation is that the variation of motion values is more spread around the moored pontoons, suggesting that the mass of the moving load significantly affects these areas more. Results from some pontoons are presented in (*Table 12*). A difference of approximately 59.2 mm is measured on A6 (moored) when loads are passing while for A8 (unmoored) only 5 mm is measured.
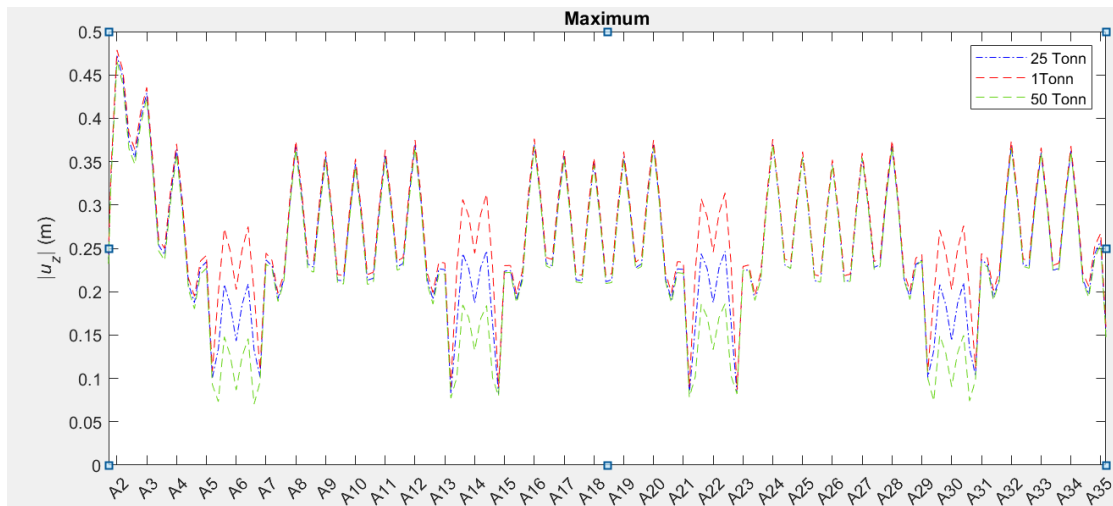
Figure 53: Results from the mass study, maximum values.
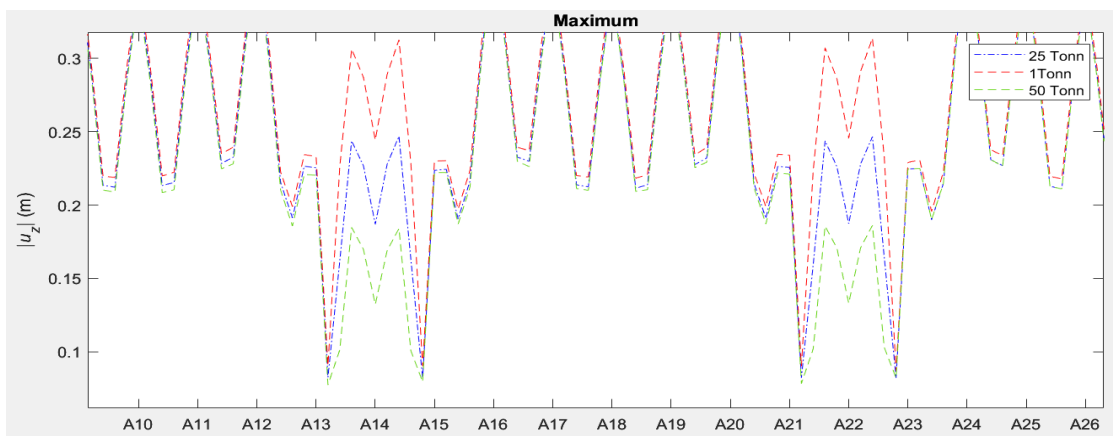

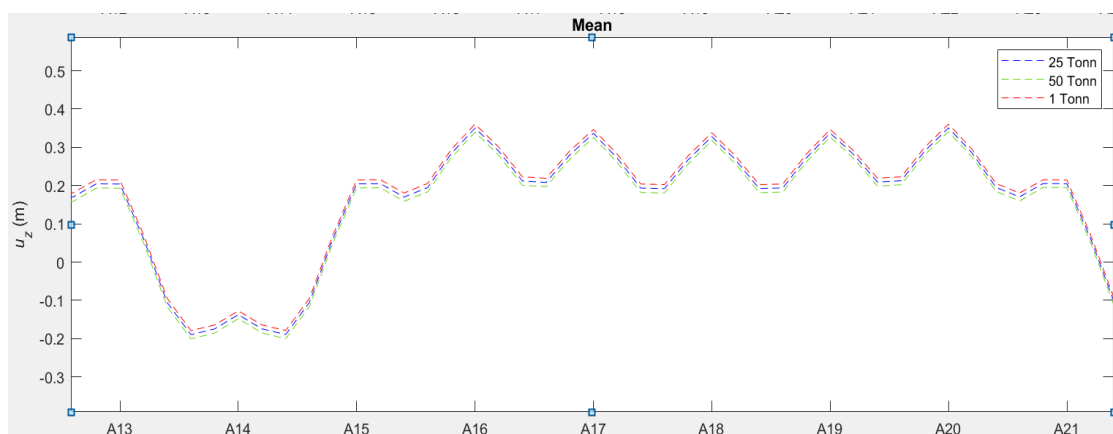Figure 54: Results from the mass study (maximum values).

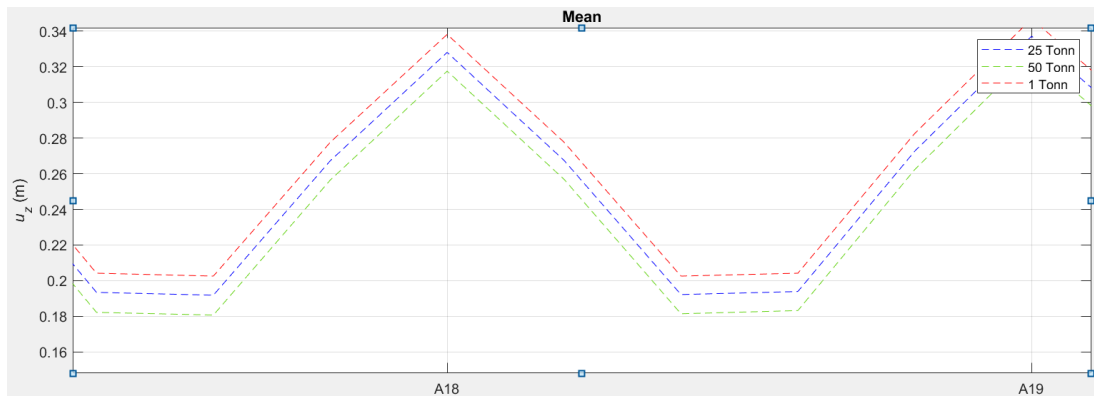Figure 55: Results from the mass study (mean values)

Figure 56: Results from the mass study (mean values)

RESULTS PRAMETERIC STUDY: MAX & MEAN VALUES FOR PONTOON A6 & A8				
PONT	UNIT	1 TONN	25 TONN	50 TONN
A6 (max	[m]	0.0866	0.1432	0.2024
A6 (mean)	[m]	-0.083	-0.094	-0.010
A8 (max)	[m]	0.364	0.369	0.374
A8 (mean)	[m]	0.347	0.347	0.359

Table 12: Max and mean values for A6 & A8

Analysis of vertical motion in time domain

The analysis of (*Figure 57)* and (*Figure 58*) revealed a clear pattern: higher loads lead to larger motions. A linear relationship was observed for girder motion. A 25-ton mass resulted in 6 cm of movement, while a 50-ton mass led to 12 cm of movement. A similar relationship could be identified for pontoon motions, with the maximum movement being 12 cm for a 100-ton mass. A similar trend was found with respect to moments seen on (Figure 59) the trend is that bigger vehicles cause grater moments. A maximum moment of 1.2 E 7 Nm can be measured. These results indicated a strong linear relationship between mass and vertical motion.
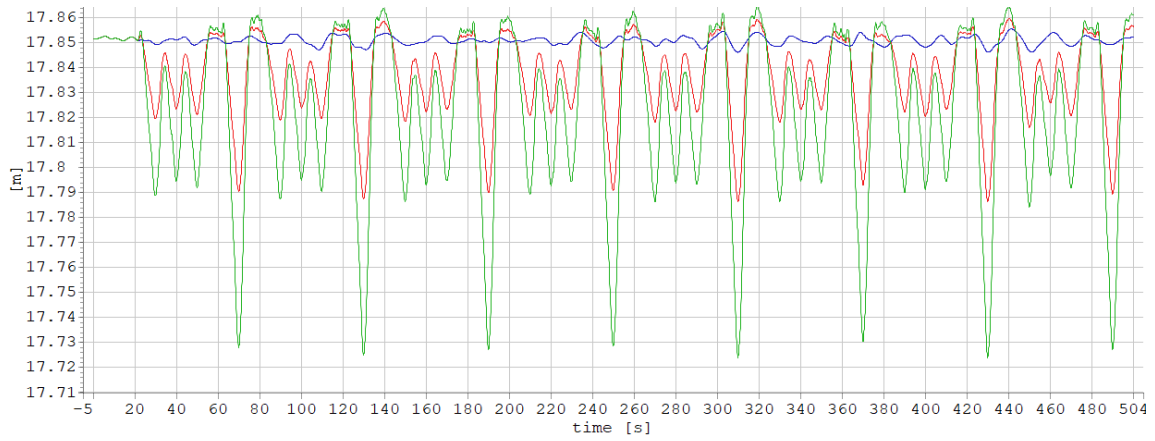
Figure 57: Vertical motion of node B2N5 (Blue = 1Ton, Red = 25 Ton, Green = 50 Ton)
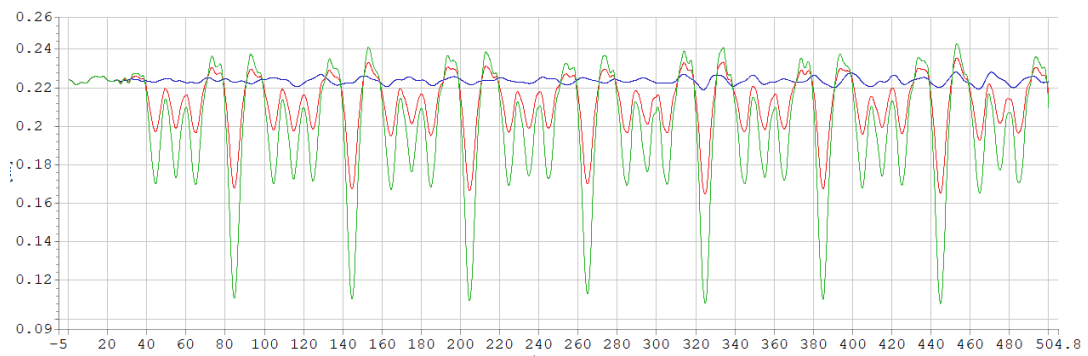
Figure 58: Vertical motion of A5 (Blue = 1Ton, Red = 25 Ton, Green = 50 Ton)
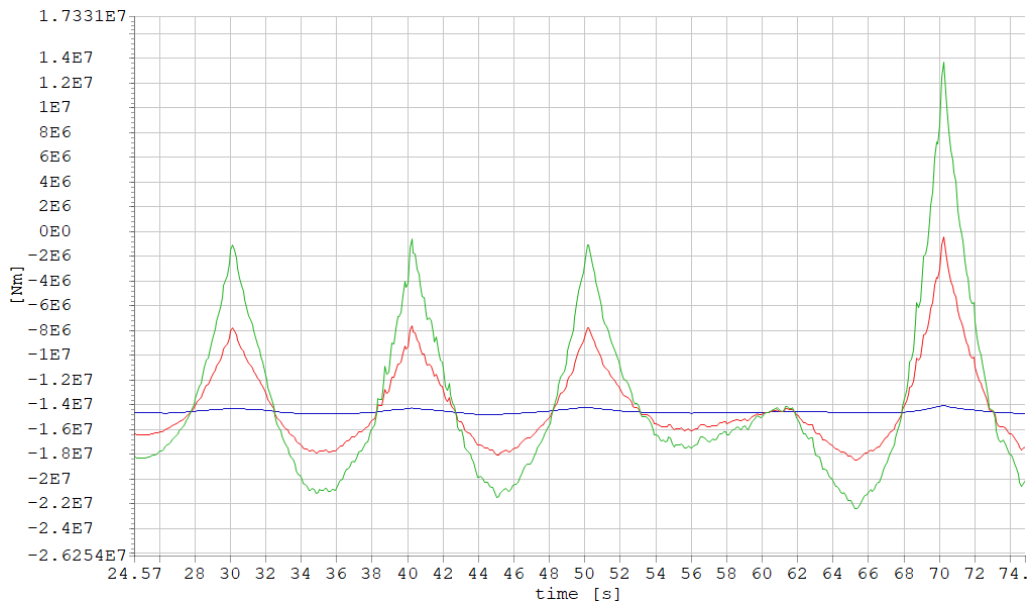
Figure 59: Moments around y axis (week) (Blue = 1Ton, Red = 25 Ton, Green = 50 Ton)

Vertical Motion: Speed Variations

This section includes an analysis of the results derived from modeling different speeds. Vehicles travel at 55 km/h and 110 km/h, and the waves are considered calm.

As seen in (Figure 60) and (Figure 63), the overall trend indicates that higher speeds lead to greater vertical motion. However, the difference is smaller compared to the variations caused by different masses. Based on (*Table 14*), a difference of 4mm and 1mm was calculated. The plots reveal a more uniform separation, with the difference between moored and unmoored pontoons being much less noticeable.
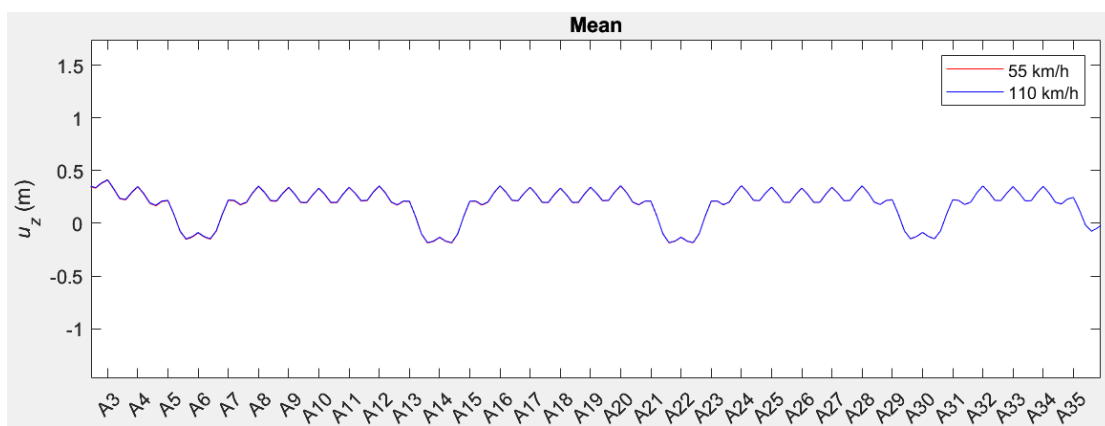
Figure 60: Vertical motion (Red = 55km/h, Blue = 110 km/h)
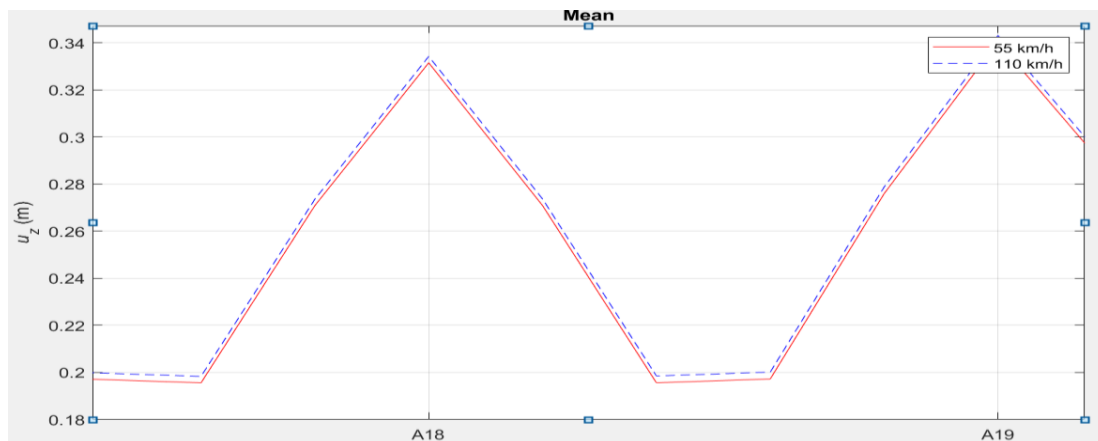
Figure 61: Vertical motion (Red = 55km/h, Blue = 110 km/h)

RESULTS SPEED TEST			
PONT	UNIT	55 km/h	110 km/h
A6 (max)	[m]	0.1150	0.1109
A6 (mean)	[m]	-0.087	-0.091
A8 (max)	[m]	0.364	0.365
A8 (mean)	[m]	0.350	0.354

Table 13:Table with data for vertical motion

Vertical Motion B5N5 in Time Domain

As seen in (*Figure 63*) and (*Figure 62*), travel speed does not impact vertical motion as significantly as vehicle mass does. A trend shows a slight increase in maximum values, but it's only 2 mm. It can be observed from the figures that when the loads have passed at high speed, some oscillations occur which do not happen at lower speeds. This phenomenon is also visible in the graphs shown in (*Figure 65*). The oscillation has been measured to have a period of 1.21 seconds. Generally, a much weaker link was observed.
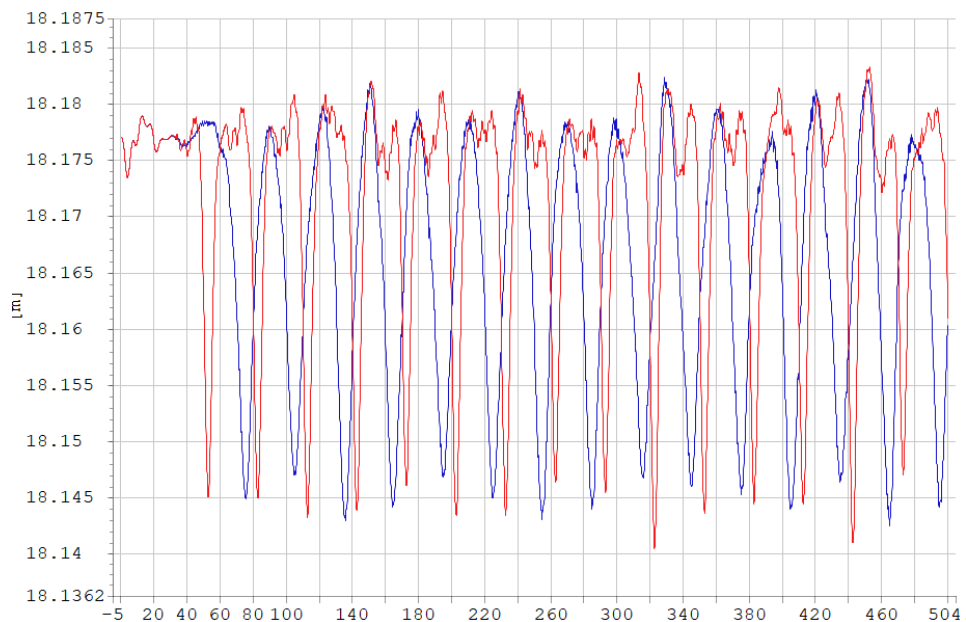
Figure 63: Vertical motion of node B5N5 (Red =110 km/h, Blue = 55 km/h)
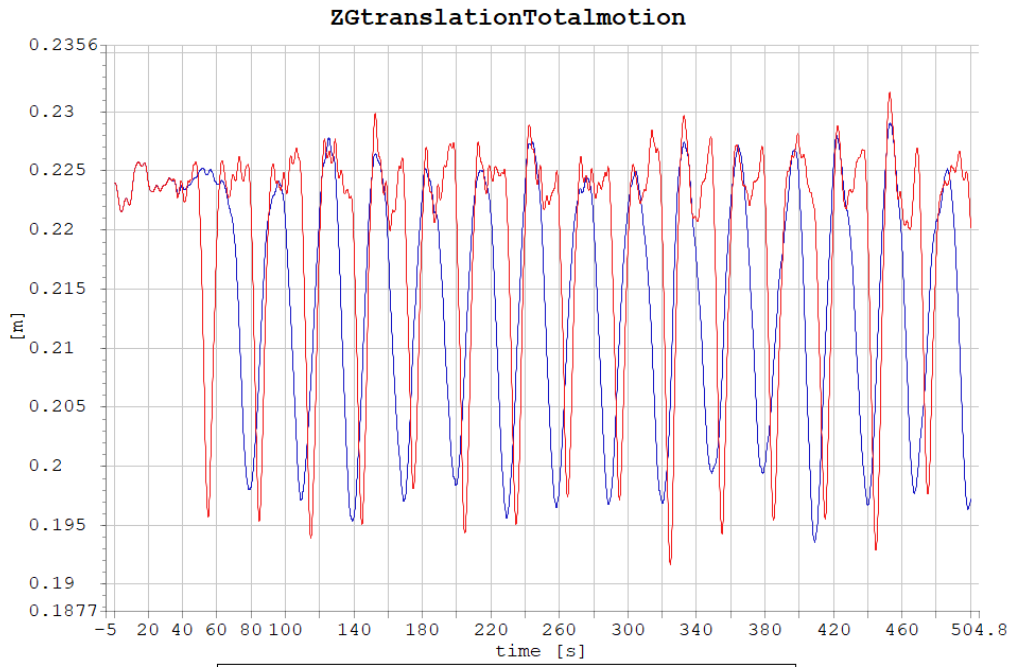
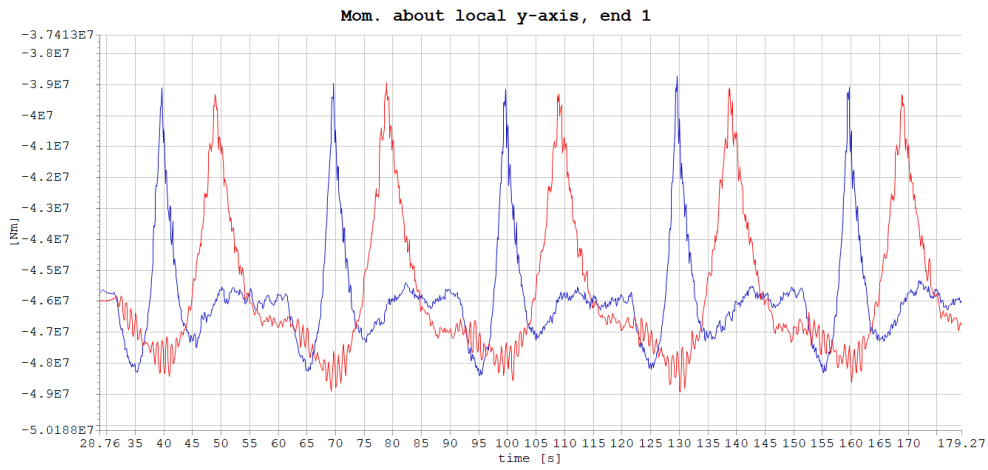Figure 64: Vertical motion of pontoon 5 (Red =110 km/h, Blue = 55 km/h)

Figure 65: Moments in y axis (week)

8.3 Stochastic Analysis: Different Traffic Scenarios

In this section, all results from the traffic conditions simulations are analyzed. Three types of traffic flow are simulated: free flow, capacity, and congestion. Waves are simulated for all three conditions, and an additional simulation of free flow without waves is also analyzed and compared. The focus will be on the vertical motion and moment. All simulations were run for at least 3600 seconds.

Global response analysis

Results from the global analysis in the position domain, with a focus on maximum and mean values, are presented in (*Figure 66*) through (*Figure 73*). Key findings are highlighted in (*Table 14*), following the figures. In general, the motions of the unmoored pontoons are greater than those of the moored ones. The largest displacement was found in A8 for the free flow condition, followed by congestion, capacity, and finally the no-wave condition. A similar trend is found for the maximum value for the moored pontoons. These results demonstrate that waves play an important role, a topic which is addressed in the following section.

VERTICAL DISPLACEMENT					
CONDITION	**UNIT**	**Unmoored**		**Moored**	
		A8-Max	**A8-Mean**	**A15-max**	**A15-mean**
Free	**[m]**	0.66	0.35	0.30	-0.19
Cap	**[m]**	0.61	0.31	0.29	-0.23
Con	**[m]**	0.63	0.30	0.30	-0.24
No	**[m]**	0.37	0.35	0.08	-0.19

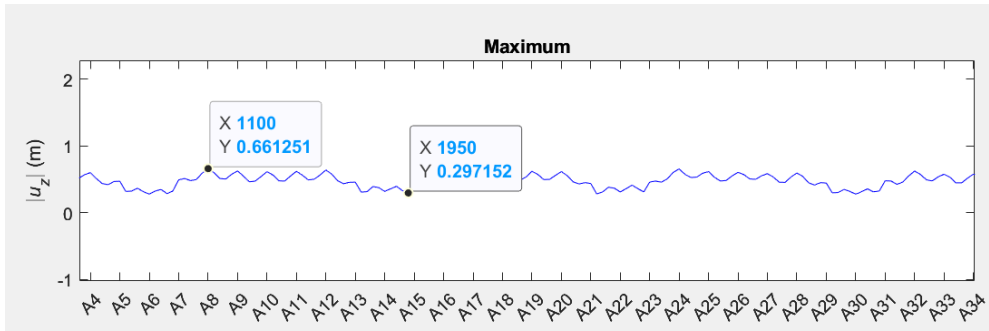Table 14: Maximum, and mean values for vertical displacement from two pontoons

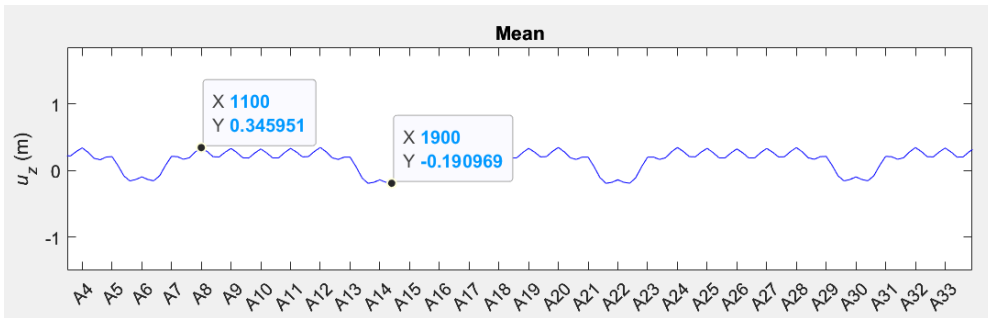Figure 66: Global maximum response for (free flow)
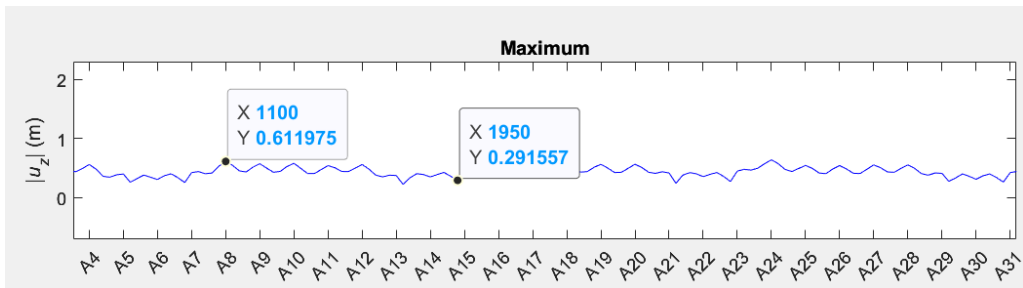

Figure 67: Global mean response (free flow)
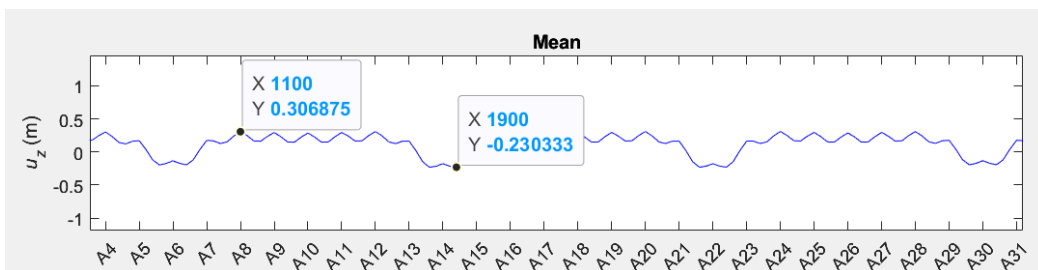

Figure 68: Global maximums motion response (capacity)

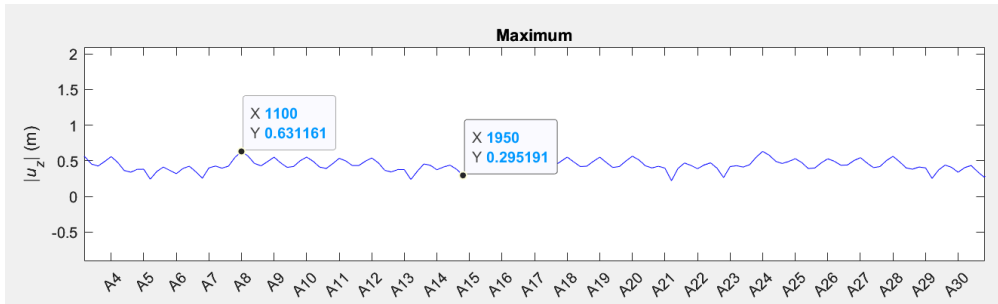Figure 69: : Global mean response (capacity)

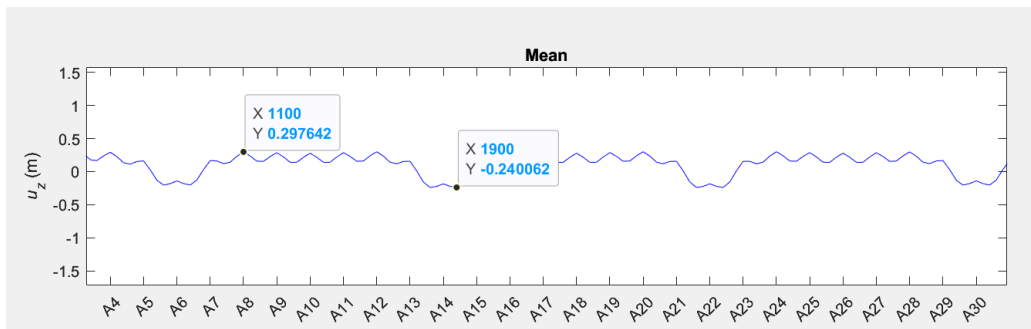Figure 70: Global maximums motion response (congestion)
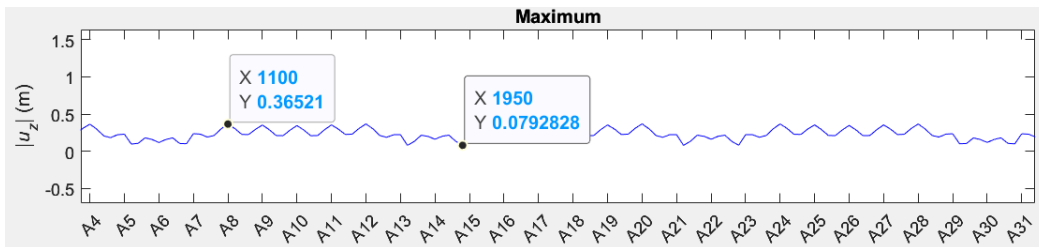

Figure 71: Global mean motion response (congestion)
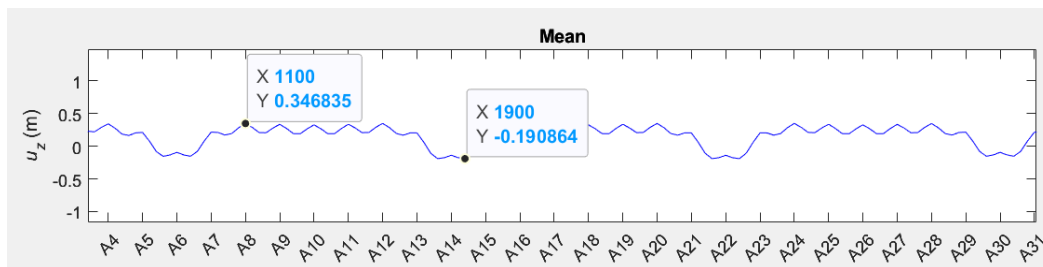

Figure 72: Global maximums motion response (calm)

Figure 73:Global mean motion response (calm)

WAVE EFFECT: FREE FLOW

In the following section, results from the free flow simulations are analyzed. As stated before, waves had a significant impact on the vertical motion of the pontoons and bridge deck. These findings are supported by results from a local analysis of nodes and pontoons in the time domain. As seen in (*Figure 74*), vertical motion is greatly affected by waves. The red lines represent motion for A8 when waves are present, and the blue lines represent calm sea conditions. The response is around 10 times the magnitude at t = 560 seconds. A similar trend can be observed in (*Figure 76*). The waves cause greater moments. (Figure 77 includes wave height. The bridge follows the waves, but the vertical motion only reaches between half and a third of the wave height.
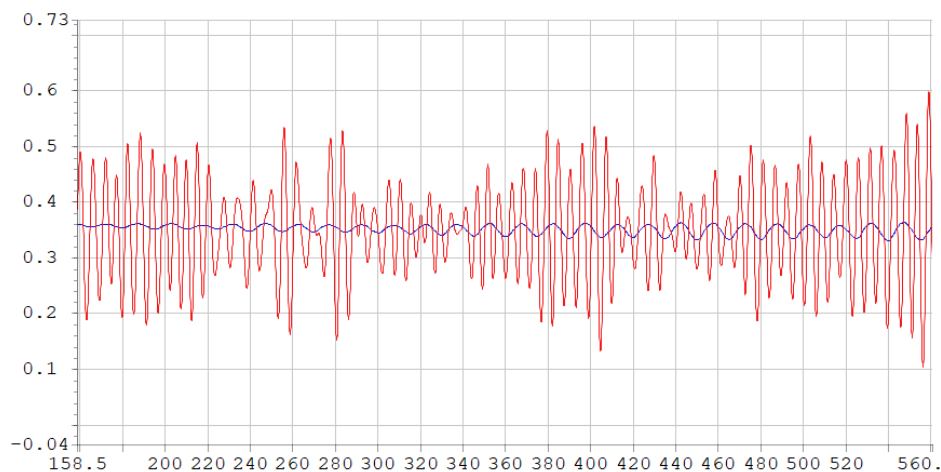

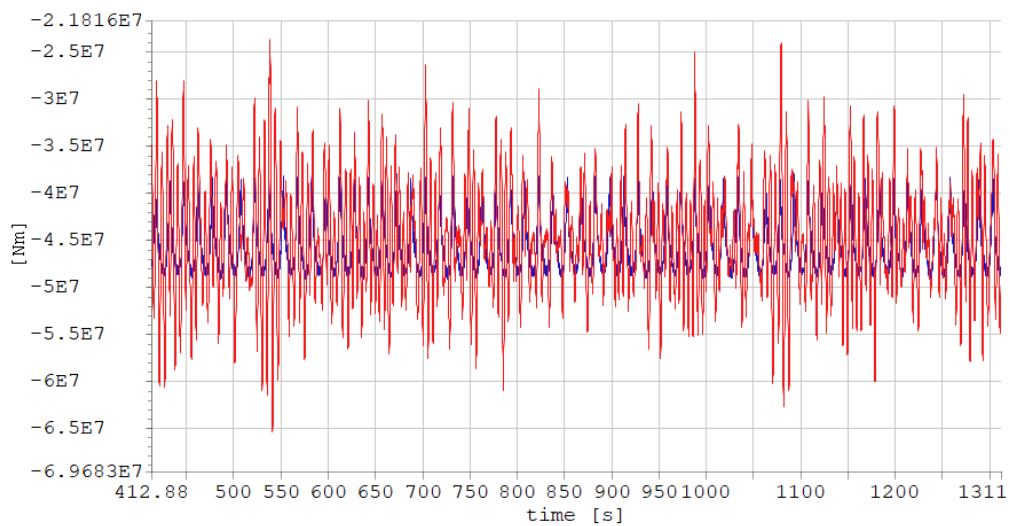Figure 74: Moments around y (week) for A8 in Free flow (Blue = calm, Red = Waves)
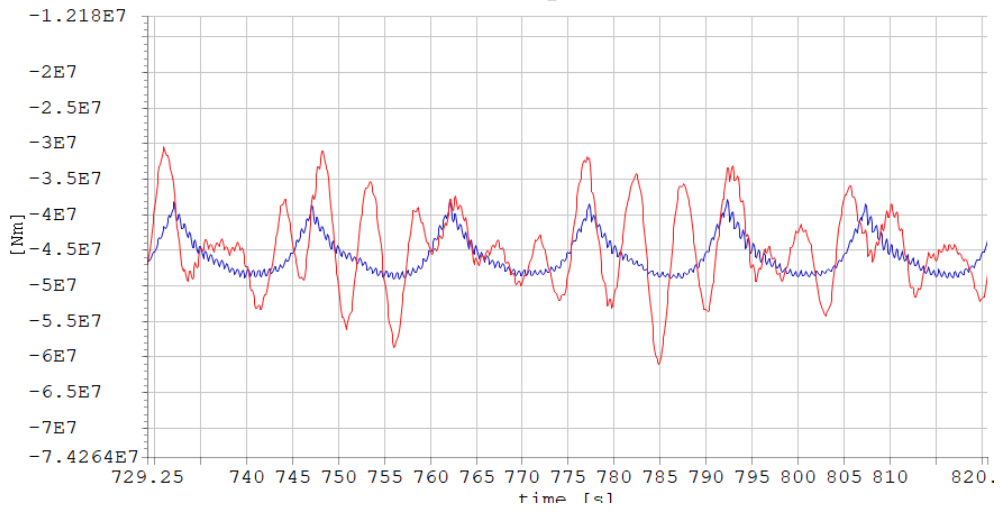

Figure 75: Moment for B2L5 (Red= Waves, Blue = Calm)

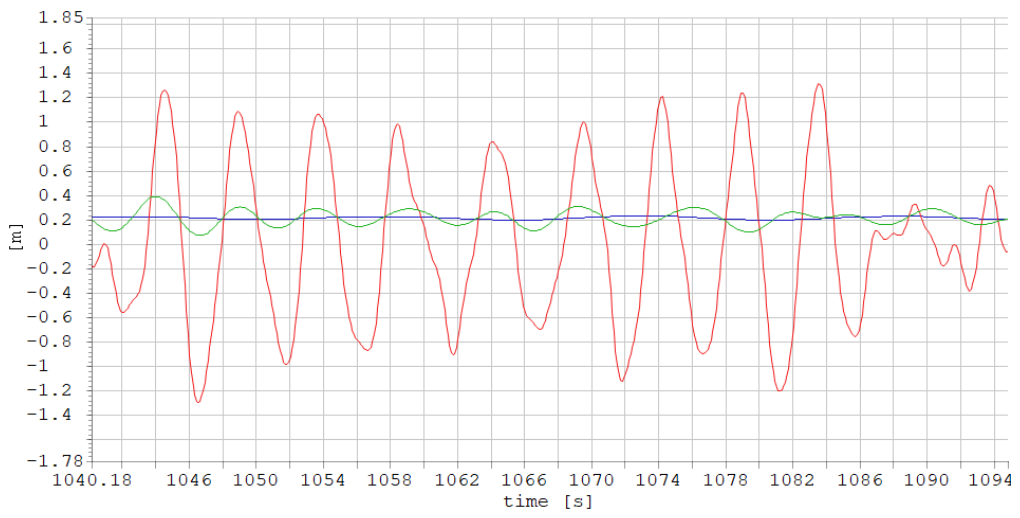Figure 76: Moment for B2L5 (Red= Waves, Blue = Calm)

Figure 77: Vertical motion P5 (Blue=calm, Green=Free, Red = wave height)

SIDE BY SIDE COMPARISON OF ALL CONDITIONS

In the figure below, all conditions are plotted. (*Figure 78*) shows that congested traffic leads to an increase in draft, with a total of 7.5 cm measured. A change in draft of approximately 1 cm is measured for the capacity flow. Similar trends can be observed in the deck displacement. Another observation is the amplitude of oscillation. In both figures, the oscillations are bigger under free traffic flow and smaller for the congested flow. One possible reason for this phenomenon is that the increase in mass causes greater inertia, thereby reducing the wave response. By studying (Figure 80), it can be seen that the pontoons' motions follow the waves, the trend is that heavier traffic loads lead to lover amplitude.
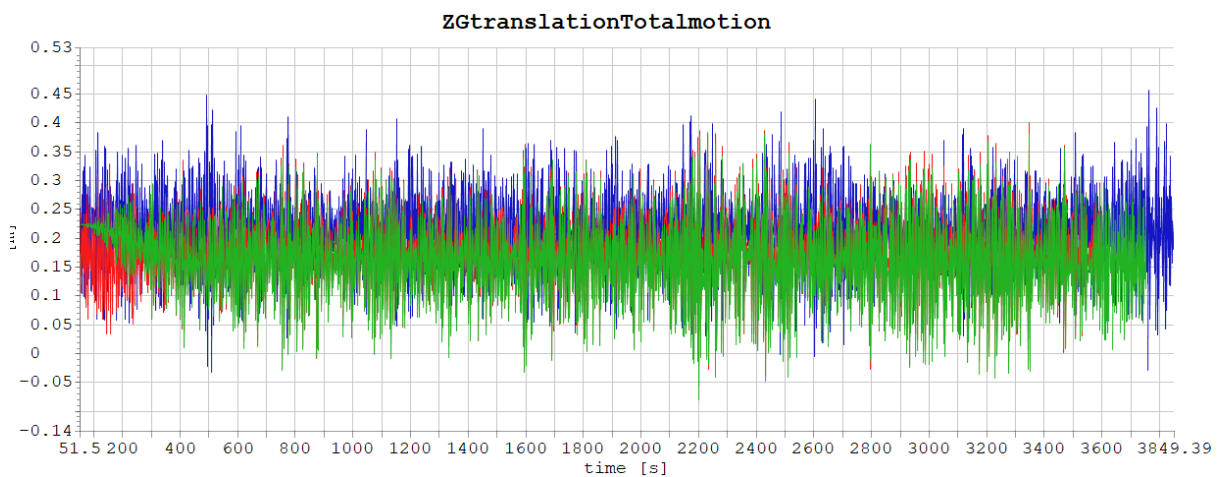

Figure 78: Vertical motion, Ponton, (Blue= free, Red = Cap, Green = Cong)
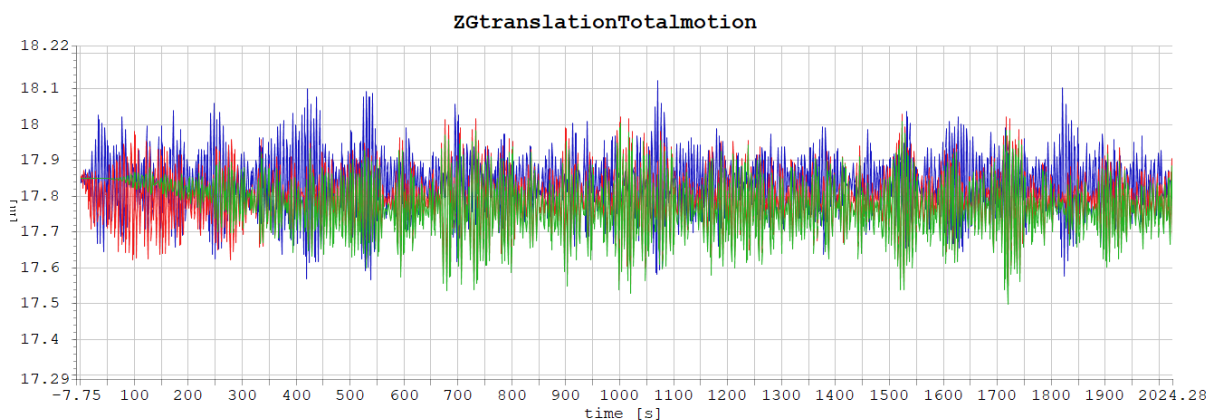
Figure 79: Vertical motion, B2N5, (Blue= free, Red = Cap, Green = Cong)
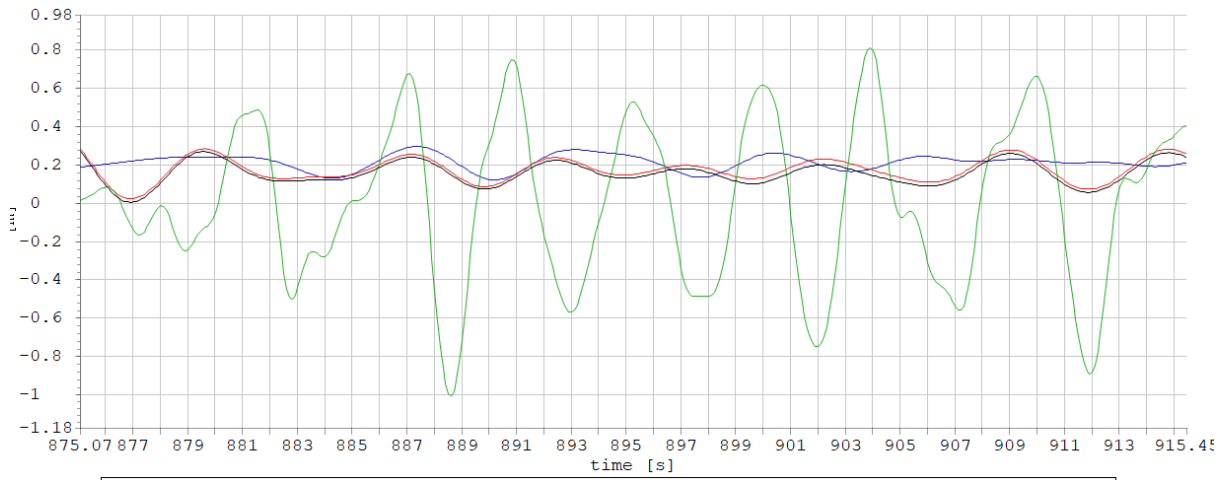
Figure 80: Vertical motion, P5, (Blue= free, Red = Cap, Green = Wave)

Moments

The moments follow a similar trend, where the free traffic flow causes the greatest peaks. This is likely because the bridge follows the waves more closely, thereby experiencing greater motion.

Figure 81:Moment around y (week) B10N7 (Blue= free, Red = Cap, Green = Cong)

Figure 82 Figure 83:Moment around y (week) B10N7 (Blue= free, Red = Cap, Green = Cong)

Chapter 9 Conclusion

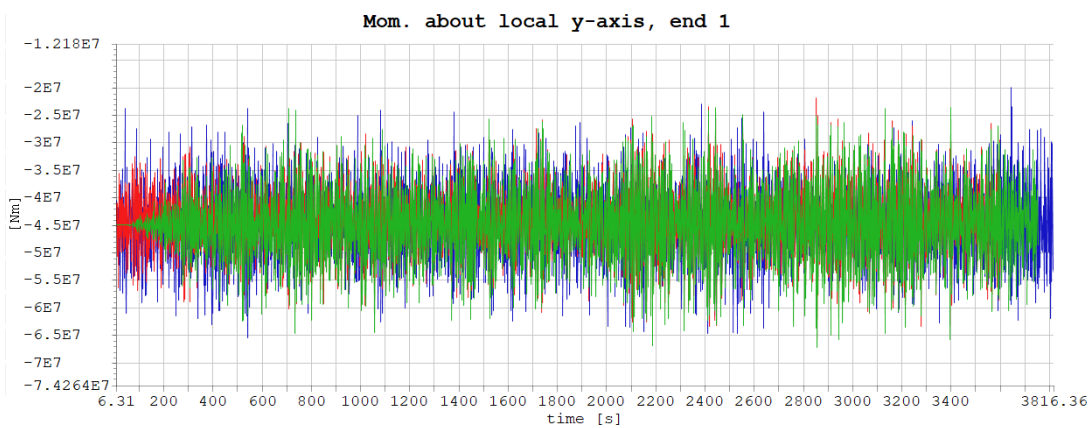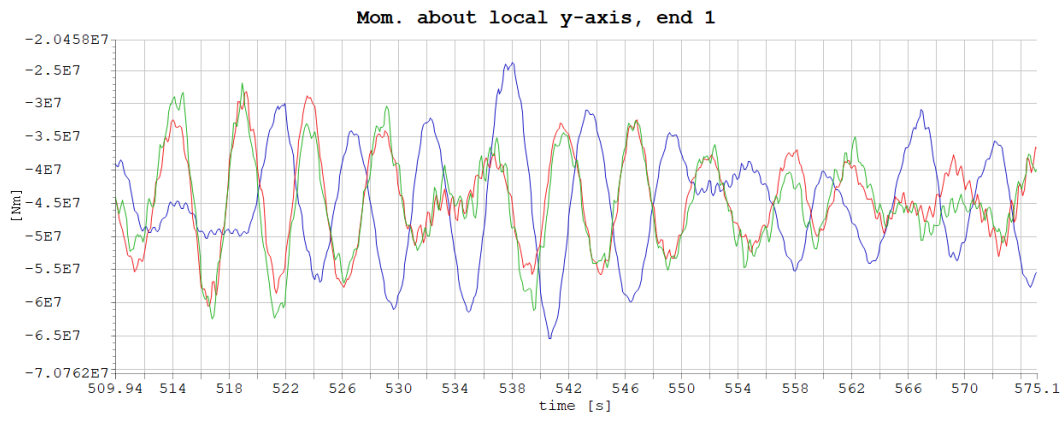The aim of this project was to investigate the relationship between vertical motion, traffic loads, and waves. To answer this question, two main studies were conducted: a parametric study of vehicle properties, and a stochastic analysis of traffic flow conditions. This project has yielded substantial data and led to key findings:

Vertical motion is mostly influenced by the mass of the traffic. However, the effect mass has on vertical motion is determined by the sea state. In calm conditions, an increase in mass leads to an increase in motion, whereas for larger waves, an increase in mass leads to less motion. In terms of peaks, an approximate 36% reduction in amplitude was found when traffic flow increased from free flow to congested when waves where present.

- Under calm sea conditions, the vertical motion is much more affected by vehicle mass than its speed. Increasing the speed from 55 km/h to 110 km/h led to an increase in vertical motion of between 1 mm and 4 mm for the moored and unmoored pontoons. Conversely, doubling the mass from 25 tons to 50 tons led to an increase in vertical motions from 6 cm to 12 cm.
- Under calm sea conditions, a linear relation was found between the vertical motion and mass of the vehicle.
- Large volumes of traffic lead to an increase in draft, with congested flow leading to a 7.5 cm increase in draft.
- When waves are present, oscillations are largest for free-flow traffic.
- For free-flow traffic, waves cause a vertical motion more than 10 times that of traffic, with the biggest difference found to be 57 cm for wave-induced motion and 3 mm for traffic-induced motion.
- A link was found between moments around the y-axis and vertical motions. However, the pattern was not fully understood. Moments are related to bending, and uniform waves lead to uniform motion.
- Simulations of dynamic traffic can be done on a coupled structural and hydrodynamic model.

The research conducted in this thesis shows how both waves and traffic contribute to the vertical motion of the bridge. In addition, the findings related to how mass affects the bridge

under different wave conditions provide new insights. While it was expected that an increase in mass would lead to an increase in motion, the findings related to the wavy sea state offer new perspectives. Hopefully this knowledge will be used for further projects.

The methods used for this project were effective and reliable, providing the desired results. Further modifications to the numerical model could be made for more precise results, including the modeling of each cross-section, as well as pontoon

Further work

In this thesis, it is demonstrated that simulating realistic traffic loads on a floating bridge is achievable, and further work shall be done to test different aspects,

- How waves with different head angles affect motion and moment
- Conduct full stop and full start simulations to study the forces arising from vehicle acc
- Simulate traffic patterns that induce resonance
- Study the effect of wind and traffic
- Test difference wave periods

Bibliography

Cook, R. D., & S, D. (2001). CONSEPTS AND APPLICATIONS OF FINITE ELEMENT ANALYSIS

DNV-GL. (2017). WADAM

Wave Analysis by Diffraction and Morison theory. *SESAM USER MANUAL*.

DNV. SIMA Documentation *2023*.

DNV. (2017). Sesam User Manual Wadam. In.

DNV. (2021). GeniE – Semisubmersible Panel and Structural (FE) Modelling. In (Vol. A7).

DNV. (2023). SIMA Documentation

Fossen, T. I. (1994). *Naviagtion and controll of vehicles*

Fu, S., & Cui, W. (2012). Dynamic responses of a ribbon floating bridge under moving loads. *Marine Structures*, *29*(1), 246-256. https://doi.org/https://doi.org/10.1016/j.marstruc.2012.06.004

Gundegjerde, S. (2017). Initial Design and Analysis of a FloatingBridge Concept.

Hasselmann

T.P.Barret

E.Bouws

H.Carlson, K. (1973). Measurements of Wind-Wace Growth and Swell Decay during the Joint North Sea Wave Project (JONSWAP).

Himite, B. (2021). Simulating Traffic Flow in Python, Implementing a microscopic traffic model

Journée, J. M. J., & Massie, W. W. (2001). *OFFSHORE HYDROMECHANICS*. Delft University of Technology.

K

Chopra, A. (1995). DYNAMICS OF STRUCTURES.

Lewandowski, E. M. (2004). *The Dynamics Of Marine Craft: Maneuvering And Seakeeping*. Word Scientific

Miao, Y.-j., Chen, X.-j., Ye, Y.-l., Ding, J., & Huang, H. (2021). Numerical modeling and dynamic analysis of a floating bridge subjected to wave, current and moving loads. *Ocean Engineering*, *225*, 108810. https://doi.org/https://doi.org/10.1016/j.oceaneng.2021.108810

Multiconsult. (2017a). *Bjørnafjorden, straight floating bridge phase 3Analysis and design (Base Case)*.

Multiconsult. (2017b). *Bjørnafjorden, straight floating bridge phase 3Analysis and design (Base Case)*.

O.M.Faltinsen. (1999). *SEA LOADS ON SHIPS AND OFFSHORE STRUCTURES*. Cambridge University Press

Ocean, S. (2017). RILEX 4.10.3 User Guid.

Porter, C. (2022). US Army float bridge system employed in Poland during DEFENDER-Europe 22.

SINTEF, o. (2017). RIFLEX 4.10.3 User Guide.

SSV. (2018). Bjørnafjorden side anchored floating bridge -independent global analyses.

Techet, A. H. (2005). 2.016 Hydrodynamics. *Potential Flow Theory*.

vegvesen, S. (18). *Bjørnafjorden side anchored floating bridge - independent*

global analyses (2017-0959).

Yang, Y. B., & Wu, C. M. (2000). DYNAMIC RESPONSE OF A HORIZONTALLY CURVED

BEAM SUBJECTED TO VERTICAL AND HORIZONTAL

MOVING LOADS.

Zhang, J., Miao, G.-p., Liu, J.-x., & Sun, W.-j. (2008). Analytical Models of Floating Bridges Subjected by Moving Loads for Different Water Depths. *Journal of Hydrodynamics, Ser. B*, *20*(5), 537-546. https://doi.org/https://doi.org/10.1016/S1001-6058(08)60092-X

Appendix A

A1 Hydrodynamic properties

ADDED MASS
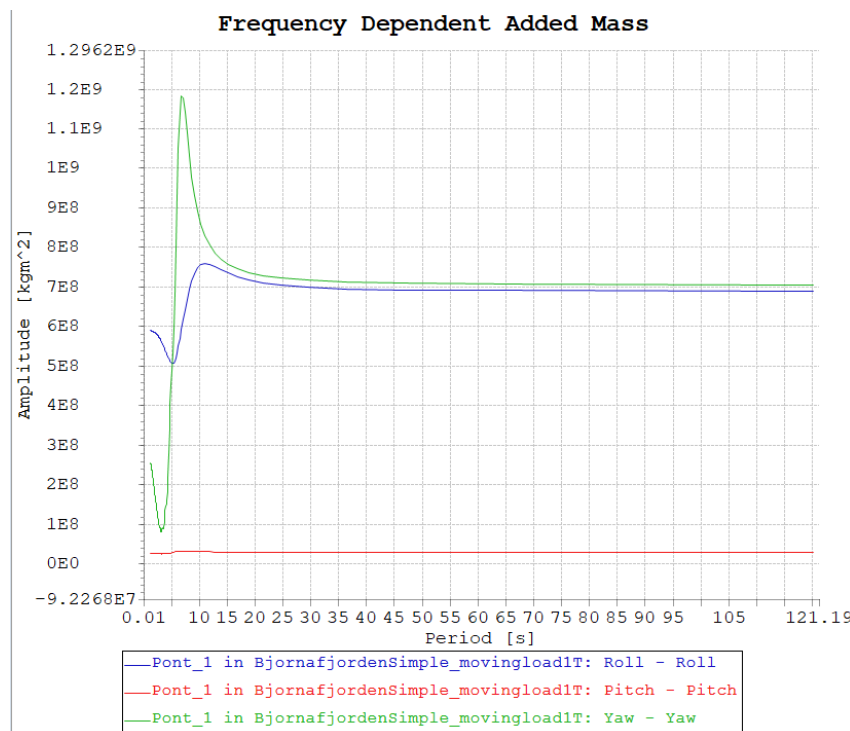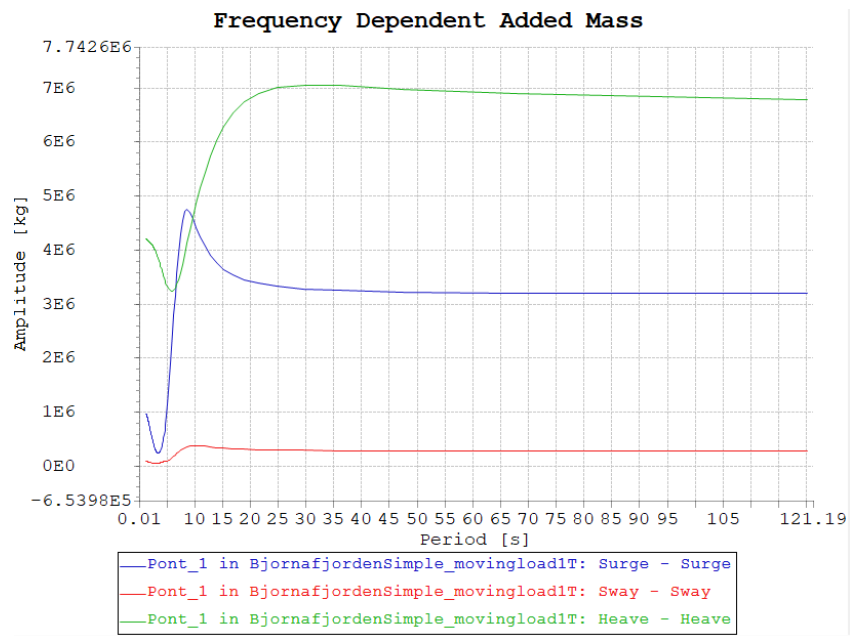
ADDED MASS INFINITY FREQUENCY

	x	y	z	rx	ry	rz
x	1.1577e+06	0.0	0.0	0.0	-2.0233e+06	0.0
y	0.0	1.0303e+05	0.0	-1.6897e+06	0.0	0.0
z	0.0	0.0	4.2478e+06	0.0	0.0	0.0
rx	0.0	-1.6907e+06	0.0	5.9223e+08	0.0	0.0
ry	-2.023e+06	0.0	0.0	0.0	2.5199e+07	0.0
rz	0.0	0.0	0.0	0.0	0.0	3.0118e+08

ADDED MASS 0 -FREQUENCY

	x	y	z	rx	ry	rz
x	3.1867e+06	0.0	0.0	0.0	-4.2317e+06	0.0
y	0.0	2.7544e+05	0.0	-5.2754e+06	0.0	0.0
z	0.0	0.0	6.7809e+06	0.0	0.0	0.0
rx	0.0	-5.275e+06	0.0	6.8863e+08	0.0	0.0
ry	-4.2317e+06	0.0	0.0	0.0	2.7876e+07	0.0
rz	0.0	0.0	0.0	0.0	0.0	7.0421e+08

DAMPING

Frequency Dependent Damping

Pont_1 in BjornafjordenSimple_movingload1T: Surge -
Pont_1 in BjornafjordenSimple_movingload1T: Sway -
Pont_1 in BjornafjordenSimple_movingload1T: Heave -

Frequency Dependent Damping

Pont_1 in BjornafjordenSimple_movingload1T: Roll - Roll
Pont_1 in BjornafjordenSimple_movingload1T: Pitch - Pitch
Pont_1 in BjornafjordenSimple_movingload1T: Yaw - Yaw

LINEAR DAMPING

	x	y	z	rx	ry	rz
x	3798.7	0.0	0.0	0.0	0.0	0.0
y	0.0	16.487	0.0	0.0	0.0	0.0
z	0.0	0.0	13966	0.0	0.0	0.0
rx	0.0	0.0	0.0	1.0598e+05	0.0	0.0
ry	0.0	0.0	0.0	0.0	2090.0	0.0
rz	0.0	0.0	0.0	0.0	0.0	5.7724e+05

HYDROSTATIC STIFFNES

```
Row  Col-1      Col-2      Col-3      Col-4      Col-5      Col-6
-----------------------------------------------------------------------
  1  0.000E+00  0.000E+00  0.000E+00  0.000E+00  0.000E+00  0.000E+00
  2  0.000E+00  0.000E+00  0.000E+00  0.000E+00  0.000E+00  0.000E+00
  3  0.000E+00  0.000E+00  6.591E+06  4.306E+03 -6.272E+02  0.000E+00
  4  0.000E+00  0.000E+00  4.306E+03  1.454E+09  2.985E+00  6.146E+01
  5  0.000E+00  0.000E+00 -6.272E+02  2.985E+00  1.018E+08  1.591E+05
  6  0.000E+00  0.000E+00  0.000E+00  0.000E+00  0.000E+00  0.000E+00
```